Abstract

In the last decades, a great progress in sedimentary provenance research has been made after the advent of detrital geochronology. Because of high closure temperature and excellent durability of zircon, the detrital-zircon U-Pb isotopic system has been most widely used, and a bounty of detrital zircon ages have thus been produced. In this study, 49,111 U-Pb ages of detrital zircons from 533 samples from the six major geological domains across the Tibetan Plateau were compiled. Multidimensional scaling (MDS) statistical analysis allowed a rigorous discrimination among detrital-zircon age spectra in numerous pre-collisional units from South Qiangtang, North Lhasa, South Lhasa and the Tethys Himalaya, and to establish the detrital-zircon age facies (DZF) characteristic of each of these domains. A test based on detrital-zircon data from stratigraphic units in the Bangong-Nujiang and Indus-Yarlung Zangbo sutures demonstrates that the identified DZF represent a reliable useful tool to effectively determine the provenance of sedimentary units contained in these two suture zones. Through this extensive compilation of zircon-age data from across the Tibetan Plateau we highlight the importance of this new approach to sedimentary provenance analysis.

Discriminating Qiangtang, Lhasa, and Himalayan sediment sources in the Tibetan Plateau by detrital-zircon U-Pb age facies

Weiwei Xue[a], Xiumian Hu[a]*, Eduardo Garzanti[c], Anlin Ma[a], Wen Lai[b],

a. State Key Laboratory of Mineral Deposits Research, School of Earth Sciences and Engineering, Nanjing University, Nanjing 210023, China

b. School of Geography and Ocean Science, Nanjing University, Nanjing 210023, China

c. Laboratory for Provenance Studies, Department of Earth and Environmental Sciences, Università di Milano-Bicocca, Milano 20126, Italy

* Corresponding author: Xiumian Hu (huxm@nju.edu.cn)

Special Issue: "Toward a big data approach for reconstructing regional to global paleogeography and tectonic histories"

Highlights

- U-Pb ages of 49,111 detrital zircons from 533 samples from the six major geological domains across the Tibetan Plateau were compiled.
- Detrital-zircon age distributions in the South Qiangtang, North Lhasa, South Lhasa, and Tethys Himalayan geological domains of the Tibetan Plateau are significantly different.
- The establishment of pre-collision detrital-zircon age facies is of great significance for identifying the sedimentary source of the suture zone

Abstract

In the last decades, a great progress in sedimentary provenance research has been made after the advent of detrital geochronology. Because of high closure temperature and excellent durability of zircon, the detrital-zircon U-Pb isotopic system has been most widely used, and a bounty of detrital zircon ages have thus been produced. In this study, 49,111 U-Pb ages of detrital zircons from 533 samples from the six major geological domains across the Tibetan Plateau were compiled. Multidimensional scaling (MDS) statistical analysis allowed a rigorous discrimination among detrital-zircon age spectra in numerous pre-collisional units from South Qiangtang, North Lhasa, South Lhasa and the Tethys Himalaya, and to establish the detrital-zircon age facies (DZF) characteristic of each of these domains. A test based on detrital-zircon data from stratigraphic units in the Bangong-Nujiang and Indus-Yarlung Zangbo sutures demonstrates that the identified DZF represent a reliable useful tool to effectively determine the provenance of sedimentary units contained in these two suture zones. Through this extensive compilation of zircon-age data from across the Tibetan Plateau we highlight the importance of this new approach to sedimentary provenance analysis.

Keywords: Tibetan Plateau; Provenance analysis; Multidimensional scaling; Detrital zircon age facies.

1 Introduction

Sedimentary provenance analysis is of key importance to understand geological evolution and reconstruct palaeotectonic and palaeogeographic settings (e.g., Dickinson, 1985). In the last decades, a great step forward has been made after the advent of detrital geochronology, which allows us to investigate the diverse time structures of source terranes, a powerful complement to the traditional petrographic or geochemical approaches that provide information on the lithological structure of parent rocks only (Garzanti et al., 2018). Because of its unique characteristics, zircon has represented the preferred target of provenance research in the last decade (Gehrels, 2011, 2014). Detrital zircon can be dated robustly and routinely at a reasonable cost and zircon-age spectra, especially if coupled with Hf isotopic fingerprinting, offer a powerful tool to identify sources characterized by specific age-windows of magmatism and crustal growth. Owing to its durability, zircon is widely preserved in ancient sandstones, where it commonly represents one of the few minerals that survived chemical dissolution during diagenesis. The durability of zircon grains, however, is not necessarily a blessing, because they can survive even multiple sedimentary cycles and age spectra may thus remain unvaried through repeated recycling episodes (e.g., Pastore et al., 2021). As a consequence, zircon ages represent the true sediment source only in the specific case of first-cycle detritus supplied directly from igneous or metamorphic basement (Dickinson et al. 2009), and in the general case can only be considered as "protosources" (Andersen et al., 2018). Other drawbacks must be kept in mind. Zircon yielding capacity is strictly controlled by bedrock lithology and sedimentary processes including weathering and hydraulic sorting (Ibañez-Mejia et al, 2018; Malusà and Garzanti, 2019). Zircon-age spectra reflect zircon-rich felsic source rocks much better than zircon-poor ones even though their outcrop area or erosion rate are limited, and other source rocks will not show up at all, including basalt, serpentinite, carbonate, or chert. Moreover, because the average percentage of zircon in sandstone is only about 0.02% (Taylor and McLennan., 1995), by focusing on zircon exclusively we shall miss information from the remaining 99.98% of the sample (Garzanti, 2016). Geochronological data from zircon grains should thus be used in conjunction with a diversified set of analytical methods and provenance tracers (Najman, 2006).

In general, samples collected from a specific depositional phase of basin evolution (e.g., tectonostratigraphic unit) display either the similar detrital-zircon U-Pb age distribution or occasionally two or even more series of similar age spectra (Schwartz et al., 2019), which are considered as “Detrital Zircon U-Pb age Facies” (henceforth DZF). Data collection and compilation of detrital zircon ages enables us to determine the DZF for any given source-rock domain or sedimentary basin. The DZF concept was first defined by LaMaskin (2012), who suggested that a unit can be considered a DZF when its detrital-zircon age distribution is characteristic and distinct from the DZF of adjacent units. Matthews et al. (2018) considered DZF, an extension of the sedimentary facies concept, as a body of genetically related rocks exhibiting reproducible detrital zircon distributions, reflecting in turn similarities in source rocks and homogenization across the sediment-routing system. The definition of DZF based on a rigorous treatment of detrital-zircon age data favours a more objective provenance interpretation. Traditional methods of handling detrital-geochronology data involve plotting a relative age probability density (PDP; Ludwing et al., 2003), kernel density estimate (KDE; Vermeesch, 2012), or a cumulative age probability diagram (CDF) (Gehrels, 2011). Then, a comparison is drawn between the KDE, PDP or CDF curve of the sedimentary unit and the curves of the potential source rocks to infer provenance. The traditional method, however, largely ignores the internal differences of potential source regions (Sircombe, 2004; Sircombe and Hazelton, 2004; Gehrels, 2011). In recent years, Multidimensional Scaling (MDS) has been frequently used to emphasize the dissimilarities among zircon age spectra (Vermeesch, 2013; Vermeesch and Garzanti, 2015; Li et al., 2020a; Ortega-Flores et al., 2021). MDS produces a map of points on which similar samples cluster closely together, and dissimilar samples plot far apart (Vermeesch, 2013) and recent studies have proved its great value for the interpretation of large datasets (Schwartz et al., 2019; Sundell and Saylor, 2021).

The aim of this article is to provide a comprehensive dataset of detrital zircon U-Pb ages from numerous sandstone units exposed in the Tibetan Plateau and the northern Himalaya. Based on those data, we discuss the time structure of each geological domain and constrain the potential sources for each exposed stratigraphic unit. The Tibetan Plateau is a product of multi-terrane amalgamation, and sedimentary provenance analysis using U-Pb ages of detrital-zircon is particularly important to explore the relationships among these terranes and the subduction-collision processes that determined their geological evolution (DeCelles et al., 2007; Hu et al., 2015; Zhu et al., 2013). Although a large amount of detrital-zircon data from the Tibetan Plateau has been published over the last 20 years, only a few studies have collected and integrated such a bounty of information. Gehrels et al. (2011) collected 13,441 zircon ages from diverse terranes of the Tibetan Plateau to characterize the signature of each. However, the zircon-age distribution in some geological domains has remained unclear because of a lack of sufficient data. Numerous recent studies on the Bangong-Nujiang and Indus-Yarlung-Zangbo suture zones of central and southern Tibet, representing key areas for research on continental subduction and collision, have provided a large amount of detrital zircon ages that better characterize not only the units contained in these two suture zones but also their potential source rocks in the adjacent Qiangtang, Lhasa, and Tethys Himalaya domains. This has created optimal conditions to build up a comprehensive detrital-zircon age compilation for source rocks all across the Tibetan Plateau.

2 Geological Background

The Tibetan Plateau is composed, from north to south, by the Hoh Xil-Songpan Ganzi, Qiangtang, Lhasa, and Tethys Himalaya geological domains (Fig. 1). The Jinshajiang suture separates the Qiangtang Block from the Hoh Xil-Songpan Ganzi terrane in the north, whereas the Bangong-Nujiang suture separates the Qiangtang Block from the Lhasa Block in the south. The Indus-Yarlung Zangbo suture separates the Lhasa Block from the Tethys Himalaya Zone in the south. The Qiangtang Block is sub-divided into the South Qiangtang and North Qiangtang terranes by the Longmu Tso-Shuanghu suture (e.g. Li Cai, 1987; Zhang et al., 2012; Zhai et al., 2016). The Lhasa Block contains two major tectonic boundaries, the Luobadui-Milashan Fault (LMF) and the Shiquanhe-Nam Tso mélange zone (SNMZ). In this study, we distinguish two terranes, North Lhasa and South Lhasa, separated by the LMF (Burg et al., 1983; England and Searle, 1986; Searle et al., 1987; Yang et al., 2009).

2.1 Longmu Tso-Shuanghu Suture

The Longmu Tso-Shuanghu suture zone (also termed Qiangtang metamorphic belt; e.g. Pullen and Kapp, 2014) is marked by a greenschist-facies sedimentary-matrix mélange exposed for ~600 km from east to west and for ~150 km from north to south in the central-western part of the Qiangtang Block (Fig. 1). Carboniferous-Triassic metasedimentary rocks and weakly deformed mafic blocks exhibit high-pressure/low-temperature metamorphic parageneses (Li, 1987; Zhai et al., 2011; Kapp et al., 2003, 2000; Pullen and Kapp, 2014). Two hypotheses have been suggested for its genesis: (1) Middle-Late Triassic collision between North Qiangtang and South Qiangtang (Li, 1987;

Zhang et al., 2006; Zhang and Tang, 2009; Zhai et al., 2016); (2) shallow-dipping southward subduction of Paleo-Tethyan oceanic lithosphere beneath the Jinshajiang suture, and detachment and exhumation along a low-angle normal fault during the latest Triassic-earliest Jurassic (Kapp et al., 2000, 2003; Pullen et al., 2008; Pullen and Kapp, 2014).

2.2 Bangong-Nujiang Suture

The Bangong-Nujiang suture zone (BNZ) extends for over 1200 km from east to west in central Tibet (Fig. 1) and consists of discontinuous ophiolitic slices, mélange, Jurassic flysch, marine conglomerate, and volcanic rocks (Fig. 2a; Allegre et al., 1984; Girardeau et al., 1984; Kapp et al., 2005; Wang et al., 2016a). Collision between the Qiangtang and Lhasa Blocks and formation of the Bangong-Nujiang suture is generally considered to have occurred by the Late Jurassic-Early Cretaceous (Girardeau et al., 1984; DeCelles et al., 2007; Kapp et al., 2007; Yan et al., 2016; Li et al., 2017a; Ma et al. 2017, 2020a; Lai et al., 2019a), although Late Cretaceous ages have also been suggested (Zhang et al., 2012, 2014; Fan et al., 2014).

Numerous stratigraphic units have been identified in the BNZ (Fig. 3). The Quhala Group, exposed in the eastern part of the BNZ, consists of quartzose sandstone, siltstone, conglomerate and mudrock deposited on a continental slope (Chen et al., 2020). The unit, dated as Late Triassic based on bivalves, was considered either as unconformably overlying the BNZ ophiolites (Chen et al., 2005) or as deposited along the North Lhasa margin (Chen et al., 2020). The conformably overlying Xihu Group consists of very-low-grade mudrock, sandstone, and pebble conglomerate. Corals and bivalves indicate deposition in shallow-marine environments during the Middle-Late Jurassic (Chen et al., 2020).

The Mugagangri Complex, exposed from east to west along the BNZ, consists of sandstone, limestone, and ultramafic blocks set in a strongly deformed siliciclastic matrix (Kapp et al., 2007; Zeng et al., 2016; Huang et al., 2017; Li et al., 2017a; Ma et al, 2020b). These deep-sea-fan deposits contain sporopollens and youngest detrital zircons indicating a Late Triassic-Middle Jurassic depositional age (Huang et al., 2017; Li et al., 2017a; Zeng et al., 2016; Ma et al., 2020b). The Gamulong Formation, consisting of deep-sea-fan conglomerate and sandstone, is exposed in the Gaize area in fault contact with the Mugagangri Complex. The youngest detrital zircons indicate a Late Jurassic depositional age (Sun et al., 2019). The Gajia Complex consists of sandstone, limestone and chert blocks set in mudrock matrix exposed in the Naqu area (Lai et al., 2017) and contains youngest detrital zircons of Early Jurassic age (~177 Ma). The Wuga Formation exposed in the Gaize area consists of sandstone, limestone, chert and pebble conglomerate deposited in hemipelagic to abyssal environments during the Late Jurassic, as indicated by the youngest detrital zircons (Li et al., 2017b).

The Yaduo Formation, exposed in the western part of the BNZ and originally assigned to the Mugagangri Complex, consists of sandstone interbedded with mudrock deposited on a deep-sea fan (Yu et al., 1990; Luo et al., 2020). The youngest detrital zircons indicate an Early Cretaceous depositional age. The Shamuluo and Dongqiao formations, unconformably overlying the Mugagangri Complex and BNZ ophiolite respectively, consist of deltaic to shallow-marine siliciclastic and limestone strata (Girardeau et al., 1984; Chen and Jiang, 2002; Deng et al., 2017; Ma et al., 2018; 2020a). Rich fossil assemblages with corals, bivalves, foraminifera, and algae indicate deposition of Shamuluo and Dongqiao formations in the Late Jurassic (Ma et al., 2018; 2020a).

2.3 South Qiangtang

The South Qiangtang terrane is comprised between the Longmu Tso-Shuanghu suture in the north and the Bangong-Nujiang suture in the south (Fig. 1). Its crystalline basement, represented by Ordovician (476-471 Ma) gneisses in the Duguer range (Pullen et al., 2011), is unconformably overlain by minor Devonian limestone, sandstone and siltstone, and by a widespread Carboniferous (anchimetamorphic quartzose sandstone, carbonate, glacigenic diamictite) to Permian (limestone, volcaniclastic sandstone) shallow-water to turbidite succession. The unconformably overlying Mesozoic succession, also widely distributed, includes Lower-Middle Triassic limestone, dolostone and sandstone (Liang et al., 2021), Upper Triassic thin-bedded limestone, shale, sandstone and minor coal beds (Wang et al., 2021c), and Jurassic shallow-marine limestone and sandstone (Ma et al., 2017; Xue et al., 2020).

2.4 North Lhasa

The North Lhasa terrane is comprised between the Bangong-Nujiang suture in the north and the Luobadui-Milashan Fault (LMF) in the south (Fig. 1). The crystalline basement is represented by Precambrian (Allegre et al., 1984) and amphibolite-facies metamorphic rocks of the Nyainqêntanglha Group exposed in the south (Zhu et al., 2013). Cambrian-Ordovician metasandstone and rhyolite nonconformably follow, overlain in turn by widespread Carboniferous-Permian very-low-grade metasedimentary rocks and glacigenic diamictite (Li et al., 2010). Upper Triassic limestone, sandstone and mudrock are locally exposed, followed by Jurassic-Lower Cretaceous shallow-marine and Upper Cretaceous continental deposits widely exposed in the north (Leier et al., 2007; Sun et al., 2017; Lai et al., 2019a; Lai et al., 2019b; Xu et al., 2021).

2.5 Luobadui-Milashan Fault (LMF)

The Luobadui-Milashan Thrust Fault extends from east to west for 1500 km across the central part of the Lhasa Block (Fig. 1), separating Carboniferous-Permian metasedimentary rocks in the hanging wall from Jurassic-Cretaceous volcano-sedimentary strata in the footwall. The Songduo eclogite and Pana garnet blueschist found along the eastern part of the LMF were suggested to represent remnants of Tethyan oceanic crust (Li et al., 2009). The LMF was consequently held to mark the boundary between the North and South Lhasa terranes, considered to be independent microcontinents during the Carboniferous-Permian (Zhu et al., 2013).

2.6 South Lhasa

The South Lhasa terrane, comprised between the Luobadui-Milashan Fault to the north and the Indus-Yarlung Zangbo suture to the south (Fig. 1), includes the Gangdese magmatic arc, the Xigaze forearc basin, and the Linzhou Basin. The Gangdese arc consists of Upper Triassic to Paleogene granitoid and volcanic rocks (Chu et al., 2006; Mo et al., 2007; Wen et al., 2008; Ji et al., 2009; Lee et al., 2009). The shallowing-upward megasequence deposited in the Xigaze forearc-basin rests stratigraphically onto the Xigaze ophiolite and consists of Aptian tuffaceous chert layers overlain by Albian-Santonian turbidites capped by Campanian-Maastrichtian shelfal, deltaic, and fluvial sediments (Wan et al., 1998; Wu et al., 2010; An et al., 2014; Orme et al., 2015; Wang et al., 2017). Exposed in the Linzhou basin to the north of Lhasa city are Middle-Upper Jurassic volcano-sedimentary rocks (Liu et al., 2018) and Upper Jurassic-Cretaceous shallow-marine carbonate to continental siliciclastic deposits (Wang et al., 2020).

2.7 Indus-Yarlung Zangbo Suture

The Indus-Yarlung Zangbo suture zone (IYSZ; Fig. 1) consists of several subparallel east/west-trending units including the Yarlung Zangbo forearc ophiolite, the Xiukang and Zongzhuo complexes, and Cenozoic conglomerates (Fig. 2b; Gansser, 1964; Tapponnier et al., 1981; Searle et al., 1987; Dupuis et al., 2006).

The 10-50-km wide Xiukang Complex is exposed south of the Yarlung Zangbo ophiolite. This mélange unit containing limestone, sandstone, and basalt blocks set in a matrix of chert and siliceous mudrock plausibly represents the deformed remnants of the Transhimalayan subduction complex (Cai et al., 2012; An et al., 2017). Fossiliferous content and youngest detrital zircons indicate deposition and subsequent deformation between the Cretaceous and the Paleocene (Tapponnier et al., 1981; Dupuis et al., 2006). The Rongmawa Formation, lying in fault contact with the Xiukang Complex and consisting of interbedded thin sandstone, siltstone, and mudrock (Orme et al., 2021), was deposited on a deep-sea fan. The youngest detrital zircons indicate a Late Cretaceous depositional age (~92-87 Ma; Hu et al., 2020). The Luogangcuo Formation, lying in fault contact with the Xiukang Complex, consists of gray-black shale, purplish-gray-green sandstone, conglomerate, with a few sandstone or chert blocks (An et al., 2018). Deposition took place on a deep-sea fan during the Late Cretaceous, as indicated by the youngest detrital zircons (92-81 Ma; An et al., 2018).

The Zongzhuo Complex, exposed farther to the south, contains blocks of chert, limestone and sandstone set in a cherty mudrock and sandstone matrix (Wu et al., 1977; Liu and Einsele, 1996; Lin, 1998). Radiolarians and youngest detrital zircons from sandstone blocks indicate a Paleocene age (Liu and Aitchison, 2002; Zhou et al., 2018). The Jiachala Formation lies in fault contact with the Zongzhuo Complex and consists of locally lenticular sandstone interbedded with shale deposited on a deep-sea fan. A Paleocene-early Eocene depositional age was suggested based on sporadic sporopollen fossils (Li et al., 2003; 2005) although the youngest detrital zircons are no younger than the Late Cretaceous (~88-84 Ma; Fu et al., 2018).

The Liuqu conglomerate, tectonically sandwiched between the Yarlung Zangbo ophiolite to the north and the Xiukang Complex to the south (Wang et al., 2010) was deposited in alluvial fan-braidplain environments (Davis et al., 2002) in the late Oligocene-early Miocene (Li et al., 2015; Leary et al., 2016).

2.8 Tethys Himalaya

The Tethys Himalaya sedimentary succession lying to the south of the Indus-Yarlung Zangbo suture zone chiefly consists of Paleozoic-Eocene siliciclastic and carbonate rocks representing the remnants of the northern Indian passive margin facing the Neotethys Ocean (Willems et al., 1996; Jadoul et al., 1998; Garzanti, 1999). A southern zone dominated by shelfal deposits passes to a northern zone characterized by largely deep-marine sediments deposited on the distal continental slope and rise (Hu et al., 2008, 2017). In the Paleocene, during the earliest stages of the impending India/Asia collision, turbidites and cherts (Sangdanlin and Zheya formations) accumulated in trench settings (An et al., 2021; Liu et al., 2021), whereas deltaic siliciclastic units fed from the Asian active margin (Enba and Zhaguo formations) were deposited in the southern Tethys Himalaya during the Eocene (Fig. 4; Li et al., 2015; Hu et al., 2012).

3 Methods and data sets

In this study we have compiled 49,111 U-Pb ages of detrital zircons from 533 samples collected in the Tibetan Plateau and published in 99 scientific articles since 2007 (Table S1). The database includes three types of information (Reference, Sample and Grain age; Fig. 5). The Reference contains information on authors, journal, year, article title, etc. The Sample contains information on sampling location (e.g., Region/Province, GPS coordinates), lithostratigraphic unit, and depositional age. The Grain age contains information on $^{206}Pb/^{238}U$, $^{207}Pb/^{235}U$, and $^{207}Pb/^{206}Pb$

isotope ratios, U/Th ratio, and ages.

3.1 Statistical methods

Non-metric multidimensional scaling (MDS) is widely used as an aid to visualize the statistical differences among a large number of samples and to objectively group samples exhibiting similar detrital zircon populations (Vermeesch, 2013; Spencer and Kirkland, 2016). In this study, sample dissimilarities were quantified by using the maximum difference between the cumulative probability density functions of each pair of samples. The D statistic of the Kolmogorov-Smirnov test is measured for each pair of samples to create a dissimilarity matrix (Vermeesch, 2013). MDS then plots samples on a Euclidean plane based on the entries of the dissimilarity matrix. The distance among samples in the MDS plot is thus proportional to sample dissimilarities based on the D statistic, and samples characterized by similar detrital-zircon age spectra will plot in the same region, thus defining a DZF (Matthews et al., 2018). Age distributions of the identified DZF were represented using kernel density estimation (KDE) plots, and age peaks were identified by detritalPy software (Sharman et al., 2018).

3.2. Criteria for the definition of DFZ

The DZF approach may contribute significantly to understanding the tectonic evolution of suture zones but strict criteria need to be followed in their definition. First of all, the boundaries among geological domains should be clearly determined. For instance, only data from units certainly deposited between the Luobadui-Milashan Fault and the Bangong-Nujiang suture were included in the three identified North Lhasa DZF. Data from stratigraphic units with controversial depositional locations, such as the Xihu and Quehala groups that may belong to either the North Lhasa terrane or the Bangong-Nujiang suture zone (Chen et al., 2020), were discarded.

Because mixed signatures are expected in post-collisional units, only pre-collisional data need to be included in the compilation. This implies that the timing of collision has to be known or assumed. We conservatively assumed the earliest possible age for the still controversial age of the Lhasa-Qiangtang collision (160 Ma; Ma et al., 2017, 2020a; Li et al., 2019) and the well constrained ~60 Ma age for the India-Asia collision (DeCelles et al., 2014; Hu et al., 2015, 2016; An et al., 2021). Only data from pre-Upper Jurassic stratigraphic units of South Qiangtang and North Lhasa, and from pre-Cenozoic units of South Lhasa and the Tethys Himalaya, were thus considered.

One stratigraphic unit may contain siliciclastic strata derived from different sources, as is the case for the Xiukang Complex (An et al., 2017) or the Sangdanlin Formation (Hu et al., 2015). Therefore, detrital-zircon ages from each unit need to be carefully analysed by MDS to verify whether the signature is homogeneous for all samples or different populations are documented by different samples. Conversely, MDS analysis may indicate that the age spectra of different stratigraphic units are homologous, and can thus be combined to define a single DZF.

3.3 Data filter rules

In our compilation, we utilized the $^{206}Pb/^{238}U$ or $^{207}Pb/^{206}Pb$ age prescribed as "best age" by the original authors, and omitted from analysis ages that were considered discordant or unreliable by them. For studies that did not define an age cut-off, we considered the $^{206}Pb/^{238}U$ ages for grains younger than 1 Ga and $^{207}Pb/^{206}Pb$ ages for grains older than 1 Ga. Concordance is not reported for $^{206}Pb/^{238}U$ ages <400 Ma because of large uncertainty in $^{206}Pb/^{207}Pb$ ages (Gehrels et al, 2011). For ages >400 Ma, only analyses with <30% discordance and <5% reverse discordance are included (Gehrels et al., 2011). Pullen et al. (2014) showed how low-n subsets (n = number of single-grain measurements per sample) of a large detrital-zircon dataset poorly reproduce the relative proportions of components of the zircon population. Therefore, we discarded samples with n <30 and most considered samples have n >>50 (Fig. 6). After data filtering, totally 45534 (527 samples) ages were analyzed (Table S2). We included in our compilation 154 samples from the Lhasa Block (12,676 ages overall, 4,879 in South Lhasa and 7,797 in North Lhasa), 70 samples from South Qiangtang (6,556 ages), 120 samples from the Tethys Himalaya (9,965 ages), 112 samples from stratigraphic units in the Bangong-Nujiang suture zone (9,324 ages), and 70 samples from stratigraphic units in the Indus-Yarlung Zangbo suture zone.

4 Detrital-zircon U-Pb age facies

Eleven detrital zircon age facies were established based on a compilation of 23,088 U-Pb published age data from the South Qiangtang, North Lhasa, South Lhasa, and Tethys Himalaya geological domains of the Tibetan Plateau.

4.1 Two detrital-zircon age facies in South Qiangtang

Two detrital-zircon age facies (DZF SQ-1, SQ-2) are identified in the South Qiangtang terrane (Table 1; Fig. 7). DZF SQ-1 (based on 49 samples from Upper Devonian Gangmacuo, Carboniferous-Permian Cameng, Zhanjin, Jipurea, Lower-Middle Triassic Tianquanshan, and Upper Triassic-Jurassic Riganpeicuo, Sewa, and Biluocuo formations) has characteristic peaks at 547, 793, 956, and 2500 Ma. This signature, similar to age spectra of pre-Triassic Tethys Himalaya sandstones, suggests original provenance from Gondwana (Gehrels et al., 2011). If recorded in Triassic-Jurassic sandstones, deposited when the Qiangtang Block had already drifted away from Gondwana, then DZF SQ-1 indicates that these zircons where largely reworked from pre-Triassic strata of South Qiangtang (Ma et al., 2017; Zhang et al., 2021).

DZF SQ-2 (based on 21 samples, mainly from the Upper Triassic Riganpeicuo, Tumengela, Gaerqin, and Jurassic Sewa, Biluocuo, and Gaacuo formations) has characteristic peaks at 176, 248, 441, and 1861 Ma. The youngest peak at ~176 Ma points at provenance from the magmatic arc developed on the southern margin of the Qiangtang Block (Li et al., 2014b; Liu et al., 2017) during northward subduction of the Bangong-Nujiang Ocean (e.g. Ma et al., 2017). Older age peaks are common to Triassic strata from the Hoh Xili-Songpan Ganzi terrane (e.g. Ding et al., 2013), reflecting extensive sediment supply from the northern Hoh Xili-Songpan Ganzi terrane during the Late Triassic to Jurassic (Gehrels et al., 2011; Ding et al., 2013).

4.2 Three detrital-zircon age facies in North Lhasa

Three detrital-zircon age facies (DZF NL-1, NL-2 and NL-3) are identified in the North Lhasa terrane, characterized by a peak at 1168-1192 Ma (Table 1; Fig. 7). DZF NL-1 (including 43 samples, mainly from the Precambrian Nyainqêntanglha Group and Cambrian Rencuo, Carboniferous-Permian Laga, Yongzhu, Laigu, and Upper Triassic Mailonggang and Duoburi formations; Fig. 3) is characterized by peaks at 538, 978, and 1192 Ma. Gehrels et al. (2011) noted that the 1192 Ma age peak also occurs in the High Himalaya, although the Upper Mesoproterozoic arc in western Australia was considered as a more likely protosource (Zhu et al., 2011; Wang et al., 2021a).

DZF NL-2 (including 5 samples from the Cambrian Nyingchi Group and Carboniferous-Permian Laga and Laigu formations) is dominated by this 1168 Ma peak, whereas DZF NL-3 (including 8 samples, mainly from the Upper Triassic Mailonggang Formation) has characteristic peaks at 304, 558, and 1170 Ma. The age peak at 304 Ma reflects Carboniferous-Permian magmatic activity on the North Lhasa terrane, whereas the 558 and 1170 Ma-aged zircons are plausibly derived from recycling of older strata (Cai et al., 2016).

4.3 Three detrital-zircon age facies in South Lhasa

Three detrital-zircon age facies (DZF SL-1, SL-2 and SL-3) are identified in the South Lhasa terrane, where Jurassic-Cretaceous peaks are dominant (Table 2; Fig. 8). DZF SL-1 (based on 37 samples mainly from the Jurassic-Cretaceous Chumulong, Shexing, Takena, Linbuzong and Yeba formations of the Linzhou Basin, and from the Cretaceous Ngamring, Padana, and Qubeiya formations of the Xigaze forearc basin) has characteristic peaks at 117, 195, 222 and 1171 Ma. The age peaks at 171-195 and 222 Ma reflect supply from the Gangdese arc to the south (Wang et al., 2020; Leier et al., 2007), whereas older zircons have a very similar distribution as pre-Jurassic detrital zircons from North Lhasa.

DZF SL-2 (including 11 samples mainly from the Cretaceous Chongdui, Ngamring, Padana, and Qubeiya formations of the eastern Xigaze forearc) has a characteristic peak at 109 Ma. DZF SL-3 (including 14 samples, mainly from the Cretaceous Dajiweng, Ngamring, Padana, and Qubeiya formations of the western Xigaze Basin) has a characteristic age peak of 92 Ma. Dominant Cretaceous ages for both DZF SL-2 and DZF SL-3 indicate direct provenance from the Gangdese arc (An et al., 2014; Orme et al., 2015).

4.4 Three detrital-zircon age facies in Tethys Himalaya

Three detrital zircon-age facies (DZF TH -1, DZF TH-2, DZF TH-3) are identified in the Tethys Himalaya, where old (500-1000 Ma) peaks are dominant (Table 2; Fig. 8). DZF TH-1 (based on 36 samples from Paleozoic and Mesozoic stratigraphic units from South Tibet) has characteristic peaks at 529 Ma and 933 Ma. These ages reveal provenance from the Pan-African belt of Gondwana (Garzanti et al., 1986; Gehrels et al. 2011). The similar age spectrum displayed by Jurassic-Cretaceous strata indicates extensive recycling of older stratigraphic units.

DZF TH-2 (based on 48 samples, mainly from the Upper Triassic Langjiexue Group, Nieru, Qulonggongba, Derirong, and Tela formations exposed in South Tibet) has characteristic peaks at 234 Ma and 520-583 Ma. Although previously held as sourced from the Lhasa Block to the north (Li et al., 2014a) or/and northwestern Australia (Cai et al., 2016; Li et al., 2016), the Langjiexue Group is here considered as an integral part of the northern Tethys Himalaya, in agreement with Wang et al. (2016b) and Meng et al. (2019). The zircon age-distribution is in fact quite similar in the Langjiexue Group as in shallow-marine Upper Triassic strata of the southern Tethys Himalaya (Qulonggongba and Derirong formations).

DZF TH-3 (based on three sample each from the Lower Cretaceous volcaniclastic Gucuo and Jiabula formations of South Tibet) has a characteristic peak at 127 Ma, reflecting the penecontemporaneous magmatism widely recorded along the Indian passive margin (Hu et al., 2010; Sciunnach and Garzanti, 2012).

5 Application of DZF in provenance analysis of suture zones

5.1 Sedimentary units in the Bangong-Nujiang suture (BNZ)

Zircon-age data from nine geological units (Mugagangri and Gajia complexes, Xihu Group, Dongqiao, Gamulong, Quehala, Shamuluo, Wuga, and Yaduo formations) were considered for MDS analysis. Fig. 9a shows how the detrital-zircon age spectrum in the Shamuluo Formation is very similar to DZF SQ-1 and SQ-2 of South Qiangtang, which is consistent with previous interpretations based on paleocurrents, sandstone composition, and detrital geochronology (Huang et al., 2017; Li et al., 2017b; Ma et al., 2018; Li et al., 2020b; Luo et al., 2020). The DZF of the Mugagangri Complex and Gamulong, Wuga, and Yaduo formations also plot close to South Qiangtang DZF in the MDS plot (Fig. 9b-9e), again consistently with previous provenance interpretations (Huang et al., 2017; Li et al., 2017b; Ma et al., 2017, 2020b; Sun et al., 2019; Luo et al., 2020). The DZF of the Quehala Group and Dongqiao Formation, instead, compare well with DZF NL-1 of North Lhasa (Fig. 9f and 9g), also in this case consistently with previous conclusions based on paleocurrents, sandstone composition and geochronological data (Chen et al., 2020; Ma et al., 2020a).

The detrital-zircon age spectrum of the Gajia Complex compares with DZF SQ-2 of South Qiangtang (Fig. 9h), in contrast with previous inferences favouring a Lhasa Block source based however on a smaller number of detrital-zircon ages and Hf isotope data (Lai et al., 2017). The Xihu Group presents two different types of age spectra, more similar to DZF NL-1 of North Lhasa in lower Xihu sandstones and to DZF SQ-2 of South Qiangtang in upper Xihu sandstones (Fig. 9i). This is in contrast with the inference by Chen et al. (2020), who suggested persistent supply from North Lhasa also in the upper Xihu Group based on northward paleocurrents. Such a different conclusion is explained by the higher proportion of magmatic zircons with synsedimentary ages of 140-150 Ma that are not included in the DZF of any potential source according to the criteria illustrated in subsection 3.2.

5.2 Sedimentary units in the Yarlung Zangbo Suture (IYSZ) and Tethys Himalaya

Zircon-age data from ten geological units (Cretaceous to Paleogene Xiukang and Zhongzhuo complexes, Jiachala, Rongmawa, Luogangcuo, Sangdanlin, Zheya, Enba, Zhaguo formations, and Liuqu Conglomerate) were considered. The detrital-zircon age distribution in the Jiachala Formation is similar to DZF SL-1 of South Lhasa (Fig. 10a), which leads us to favour provenance from the South Lhasa terrane consistently with previous interpretations based on paleocurrents, sandstone composition, and detrital zircon U-Pb and Lu-Hf data (Fu et al., 2018; Wang et al., 2021b). The Zongzhuo Complex, Rongmawa and Luogangcuo formations also have detrital-zircon age distributions similar as DZF SL-1 and SL-2 (Fig. 10b-10d), consistently with previously interpreted provenance from South Lhasa (Sun et al., 2011; Cai et al., 2012; An et al., 2018; Zhou et al., 2018; Laskowski et al., 2019; Orme et al., 2021). The Xiukang Complex presents two different types of age spectra (Fig. 10e), with samples similar to either DZF SL-1 of South Lhasa or DZF TH-2 of the Tethys Himalaya, confirming dual sources for this unit (An et al., 2017). Two types of age spectra are also observed for sandstones of the syncollisional Sangdanlin Formation, one being similar as DZF SL-1 and SL-2 of South Lhasa and the other one as DZF TH-1 of the Tethys Himalaya (Fig. 10h). The Sangdanlin Formation did in fact receive detritus from both colliding northern India and southern Asian margins (DeCelles et al., 2014; Hu et al., 2015; An et al., 2021).

Post-collisional units include the Paleocene Zheya Formation deposited on top of the Sangdanlin Formation and the Eocene Enba and Zhaguo formations deposited on top of the Tethys Himalaya succession. These three units yielded detrital-zircon age distributions similar to DZF SL-1 and SL-2 of South Lhasa (Fig. 10f and 10g), consistently with previous provenance interpretations (Hu et al., 2012; DeCelles et al., 2014; Li et al., 2015). Finally, the detrital-zircon age distribution of the younger Liuqu conglomerate is similar to DZF SL-1 and SL-2 of South Lhasa (Fig. 10i), although northward paleocurrent and clast lithology rather indicates provenance from the Indus-Yarlung Zangbo suture zone and Tethys Himalaya (Leary et al., 2016). This inconsistency is explained with reworking of the Xiukang Complex and Indus-Yarlung Zangbo suture zone mélange (Leary et al., 2016) (Fig. 10e).

5.3. Testing the validity of the DZF approach

The advantages of the DZF approach are here outlined by using as examples the Wuga and Rongmawa formations of the Bangong-Nujiang and Indus-Yarlung Zangbo suture zones. By the conventional approach, the averaged KDE curves considering all pre-Cenozoic detrital-zircon ages from South Qiangtang and North Lhasa would be compared to the age distribution obtained from sandstones of the Wuga Formation (Li et al., 2017b). As a result, no close correspondence would be found between the wide cluster ranging from 150-500 Ma characteristic of the Wuga Formation with either the South Qiangtang or North Lhasa curves (Fig. 11a). However, if two distinct DZF are defined for South Qiangtang, then the age spectrum of the Wuga Formation would find a correspondence with DZF SQ-2 (Figs. 9c and 11b), indicating provenance from South Qiangtang, consistently with the previous interpretation (Li et al., 2017b).

Similarly, no close comparison is found if averaged KDE curves including all pre-Cenozoic detrital-zircon ages from South Lhasa and the Tethys Himalaya are compared with the age spectrum of the Rongmawa Formation (Fig. 12a). Although the age peak between 516 and 560 Ma compares well with the Tethys Himalaya (Fig. 12a), both South Lhasa and Tethys Himalaya apparently lack age peaks at 1175 Ma. However, if DZF are differentiated, then the age spectrum of the Rongmawa Formation is seen to compare well with DZF SL-1 (Figs. 10b and 12b), indicating that the Rongmawa Formation was chiefly supplied from the Lhasa Block (Cai et al., 2012; Laskowski et al., 2019; Orme et al., 2021).

The DZF approach thus proves to be superior to the conventional approach insofar it allows to consider fundamental differences within different potential source regions. Moreover, an averaged KDE curve based on a pool of heterogeneous data derived from inhomogeneously sampled units is prone to provide a distorted image of potential source-rock domains. The DZF is able to provide a more accurate image of the time structure of source rocks and hence proves to be a more powerful tool for provenance analysis.

5.4. First cycle vs. recycled zircon grains

Durable zircon grains can survive multiple recycling and this represents a big problem in provenance research. Apart from the special case of zircon crystals derived from volcanic sources active during the time of deposition, it is generally impossible to determine whether a zircon grain is derived first-cycle from igneous or metamorphic rocks or recycled from siliciclastic strata. For this reason, the DZF approach should be always integrated with other provenance tracers. Potential pitfalls are many. For instance, although the zircon-age spectrum of the Gamulong Formation compares well with DZF SQ-2 of South Qiangtang (Fig. 9b), sandstones of the Gamulong Formation contain abundant sedimentary rock fragments, indicating recycling of the Mugagangri Group of the Bangong-Nujiang suture zone (Sun et al., 2019).

The opposite problem may be caused by an abundance of zircons derived from a volcanic source active at the time of deposition. The Upper Xihu Group contains a high proportion of synsedimentary magmatic zircons aged as 150-140 Ma, which causes a mismatch with the DZF used for comparison that do not contain such a peak (section 5.1; Fig. 9i). This problem is commonly encountered in post-collision provenance analysis. For instance, many samples from the Lower Cretaceous Duoni and Duba formations of the North Lhasa terrane do not match the DZF of either North Lhasa or South Qiangtang (Fig. 13a and 13c) because they have a high proportion of synsedimentary magmatic zircon aged as 100-125 Ma (Fig. 13b and 13d).

Conclusion

Detrital-zircon age distributions in the South Qiangtang, North Lhasa, South Lhasa, and Tethys Himalayan geological domains of the Tibetan Plateau are significantly different. Each domain is characterized by distinct detrital-zircon age facies, identified by using the multidimensional scaling

(MDS) technique: two for South Qiangtang (DZF SQ-1, SQ-2) and three each for North Lhasa (DZF NL-1, NL-2, NL-3), South Lhasa (DZF SL-1, SL-2, SL-3), and the Tethys Himalaya (DZF TH-1, TH-2, TH-3). These 11 detrital zircon age facies effectively identify sandstone provenance in 19 stratigraphic units in the Bangong Nujiang and Yarlung Zangbo suture zones and of the Tethys Himalaya.

Declaration of Competing Interest

The authors declare that they have no known competing financial interests or personal relationships that could have appeared to influence the work reported in this paper.

Acknowledgements

We thank Chao Li, Dingjun Wen, Xiaoji Zhang and Yingdi Pan for assistance in collecting literature data. This work was financially supported by the Natural Science Foundation of China (42050102 and 41888101) and by the program B for Outstanding PhD candidate of Nanjing University.

References

Allégre, C.J., Courtillot, V., Tapponnier, P., Hirn, A., Mattauer, M., Coulon, C., Jaeger, J.J., Achache, J., Schärer, U., Marcoux, J., Burg, J.P., Girardeau, J., Armijo, R., Gariépy, C., Göpel, C., Tindong, L., Xuchang, X., Chenfa, C., Guangqin, L., Baoyu, L., Jiwen, T., Naiwen, W., Guoming, C., Tonglin, H., Xibin, W., Wanming, D., Huaibin, S., Yougong, C., Ji, Z., Hongrong, Q., Peisheng, B., Songchan, W., Bixiang, W., Yaoxiu, Z. and Xu, R., 1984. Structure and evolution of the Himalaya–Tibet orogenic belt. Nature, 307(5946): 17-22.

An, W., Hu, X. and Garzanti, E., 2017. Sandstone provenance and tectonic evolution of the Xiukang Mélange from Neotethyan subduction to India–Asia collision (Yarlung-Zangbo suture, south

Tibet). Gondwana Research, 41: 222-234.

An, W., Hu, X. and Garzanti, E., 2018. Discovery of Upper Cretaceous Neo-Tethyan trench deposits in south Tibet (Luogangcuo Formation). Lithosphere, 10(3): 446-459.

An, W., Hu, X., Garzanti, E., BouDagher-Fadel, M.K., Wang, J. and Sun, G., 2014. Xigaze forearc basin revisited (South Tibet): Provenance changes and origin of the Xigaze Ophiolite. GSA Bulletin, 126(11-12): 1595-1613.

An, W., Hu, X., Garzanti, E., Wang, J.-G. and Liu, Q., 2021. New Precise Dating of the India-Asia Collision in the Tibetan Himalaya at 61 Ma. Geophysical Research Letters, 48(3): e2020GL090641.

Andersen, T., Elburg, M.A., van Niekerk, H.S. and Ueckermann, H., 2018. Successive sedimentary recycling regimes in southwestern Gondwana: Evidence from detrital zircons in Neoproterozoic to Cambrian sedimentary rocks in southern Africa. Earth-Science Reviews, 181: 43-60.

Burg, J.-P., Proust, F., Tapponnier, P. and Ming, C.G., 1983. Deformation phases and tectonic evolution of the Lhasa block (southern Tibet, China). Eclogae Geologicae Helvetiae, 76(3): 643-665.

Cai, F., Ding, L., Laskowski, A.K., Kapp, P., Wang, H., Xu, Q. and Zhang, L., 2016. Late Triassic paleogeographic reconstruction along the Neo–Tethyan Ocean margins, southern Tibet. Earth and Planetary Science Letters, 435: 105-114.

Cai, F., Ding, L., Leary, R.J., Wang, H., Xu, Q., Zhang, L. and Yue, Y., 2012. Tectonostratigraphy and provenance of an accretionary complex within the Yarlung–Zangpo suture zone, southern Tibet: Insights into subduction–accretion processes in the Neo-Tethys. Tectonophysics, 574-575: 181-192.

Chen, Y. L., Jiang Y. S., 2002. Age and significance of volcanic rock of Early Cretaceous in the Bange-Qielicuo area in Tibet. Journal of Geomechanics, 8(1): 43-49. (in Chinese with English abstract).

Chen, Y. L., Zhang, K. Z., Li, G. Q., Nimaciren., Zhao, S. R. and Chen, G. R., 2005. Discovery of an uniformity between the Upper Triassic Quehala Group and its underlying rock series in the central segment of the Bangong Co-Nujiang Junction zone, Tibet, China. Geological Bulletin of China, 24(7): 621-624. (in Chinese with English abstract).

Chen, Y., Ding, L., Li, Z., Laskowski, A.K., Li, J., Baral, U., Qasim, M. and Yue, Y., 2020. Provenance analysis of Cretaceous peripheral foreland basin in central Tibet: Implications to precise timing on the initial Lhasa-Qiangtang collision. Tectonophysics, 775: 228311.

Chu, M.-F., Chung, S.-L., Song, B., Liu, D., O'Reilly, S.Y., Pearson, N.J., Ji, J. and Wen, D.-J., 2006. Zircon U-Pb and Hf isotope constraints on the Mesozoic tectonics and crustal evolution of southern Tibet. Geology, 34(9): 745-748.

Davis, A.M., Aitchison, J.C., Luo, H. and Zyabrev, S., 2002. Paleogene island arc collision-related conglomerates, Yarlung–Zangbo suture zone, Tibet. Sedimentary Geology, 150(3): 247-273.

DeCelles, P.G., Kapp, P., Ding, L. and Gehrels, G.E., 2007. Late Cretaceous to middle Tertiary basin evolution in the central Tibetan Plateau: Changing environments in response to tectonic partitioning, aridification, and regional elevation gain. GSA Bulletin, 119(5-6): 654-680.

DeCelles, P.G., Kapp, P., Gehrels, G.E. and Ding, L., 2014. Paleocene-Eocene foreland basin evolution in the Himalaya of southern Tibet and Nepal: Implications for the age of initial India-Asia collision. Tectonics, 33(5): 824-849.

Deng, J. H., Yuan, Z. G., Yu, J., Du, C. F., Tang, Z. Y., Sun, S. L., Lv, X., Zhong W., Wan C. and Zhong, J. J., 2017. New discovery of the basal conglomerate in the Upper Jurassic-Lower Cretaceous Shamuluo Formation in western part of Bangong Lake-Nujiang suture zone and its geological significance. Geological Review, 63(2): 302-309. (in Chinese with English abstract).

Dickinson, W.R., 1985. Interpreting Provenance Relations from Detrital Modes of Sandstones. In: G.G. Zuffa (Editor), Provenance of Arenites. Springer Netherlands, Dordrecht, pp. 333-361.

Dickinson, W.R., Lawton, T.F. and Gehrels, G.E., 2009. Recycling detrital zircons: A case study from the Cretaceous Bisbee Group of southern Arizona. Geology, 37(6): 503-506.

Ding, L., Yang, D., Cai, F.L., Pullen, A., Kapp, P., Gehrels, G.E., Zhang, L.Y., Zhang, Q.H., Lai, Q.Z., Yue, Y.H. and Shi, R.D., 2013. Provenance analysis of the Mesozoic Hoh-Xil-Songpan-Ganzi turbidites in northern Tibet: Implications for the tectonic evolution of the eastern Paleo-Tethys Ocean. Tectonics, 32(1): 34-48.

Dupuis, C., Hébert, R., Dubois-Côté, V., Guilmette, C., Wang, C.S. and Li, Z.J., 2006. Geochemistry of sedimentary rocks from mélange and flysch units south of the Yarlung Zangbo suture zone, southern Tibet. Journal of Asian Earth Sciences, 26(5): 489-508.

England, P. and Searle, M., 1986. The Cretaceous-tertiary deformation of the Lhasa Block and its implications for crustal thickening in Tibet. Tectonics, 5(1): 1-14.

Fan, J.-J., Li, C., Xie, C.-M. and Wang, M., 2014. Petrology, geochemistry, and geochronology of the Zhonggang ocean island, northern Tibet: implications for the evolution of the Banggongco–Nujiang oceanic arm of the Neo-Tethys. International Geology Review, 56(12): 1504-1520.

Fu, H., Hu, X., Crouch, E.M., An, W., Wang, J. and Garzanti, E., 2018. Upper Cretaceous trench deposits of the Neo-Tethyan subduction zone: Jiachala Formation from Yarlung Zangbo suture zone in Tibet, China. Science China Earth Sciences, 61(9): 1204-1220.

Gansser, A., 1964. Geology of the Himalayas. Wiley Interscience, New York.

Garzanti, E., 1999. Stratigraphy and sedimentary history of the Nepal Tethys Himalaya passive margin. Journal of Asian Earth Sciences, 17(5): 805-827.

Garzanti, E., 2016. From static to dynamic provenance analysis—Sedimentary petrology upgraded. Sedimentary Geology, 336: 3-13.

Garzanti, E., Casnedi, R. and Jadoul, F., 1986. Sedimentary evidence of a Cambro-Ordovician orogenic event in the northwestern Himalaya. Sedimentary Geology, 48(3): 237-265.

Garzanti, E., Vermeesch, P., Rittner, M. and Simmons, M., 2018. The zircon story of the Nile: Time-structure maps of source rocks and discontinuous propagation of detrital signals. Basin Research, 30(6): 1098-1117.

Gehrels, G., 2011. Detrital Zircon U-Pb Geochronology: Current Methods and New Opportunities, Tectonics of Sedimentary Basins, pp. 45-62.

Gehrels, G., 2014. Detrital Zircon U-Pb Geochronology Applied to Tectonics. Annual Review of Earth and Planetary Sciences, 42(1): 127-149.

Gehrels, G., Kapp, P., DeCelles, P., Pullen, A., Blakey, R., Weislogel, A., Ding, L., Guynn, J., Martin, A., McQuarrie, N. and Yin, A., 2011. Detrital zircon geochronology of pre-Tertiary strata in the Tibetan-Himalayan orogen. Tectonics, 30(5).

Girardeau, J., Marcoux, J., Allègre, C.J., Bassoullet, J.P., Youking, T., Xuchang, X., Yougong, Z. and Xibin, W., 1984. Tectonic environment and geodynamic significance of the Neo-Cimmerian Donqiao ophiolite, Bangong-Nujiang suture zone, Tibet. Nature, 307(5946): 27-31.

Hu, X., An, W., Garzanti, E. and Liu, Q., 2020. Recognition of trench basins in collisional orogens:

Insights from the Yarlung Zangbo suture zone in southern Tibet. Science China Earth Sciences, 63(12): 2017-2028.

Hu, X., Garzanti, E., Moore, T. and Raffi, I., 2015. Direct stratigraphic dating of India-Asia collision onset at the Selandian (middle Paleocene, 59 ± 1 Ma). Geology, 43(10): 859-862.

Hu, X., Garzanti, E., Wang, J., Huang, W., An, W. and Webb, A., 2016. The timing of India-Asia collision onset–Facts, theories, controversies. Earth-Science Reviews, 160: 264-299.

Hu, X., Jansa, L., Chen, L., Griffin, W.L., O'Reilly, S.Y. and Wang, J., 2010. Provenance of Lower Cretaceous Wölong Volcaniclastics in the Tibetan Tethyan Himalaya: Implications for the final breakup of Eastern Gondwana. Sedimentary Geology, 223(3): 193-205.

Hu, X., Jansa, L. and Wang, C., 2008. Upper Jurassic–Lower Cretaceous stratigraphy in south-eastern Tibet: a comparison with the western Himalayas. Cretaceous Research, 29(2): 301-315.

Hu, X., Li, J., An, W. and Wang J. G., 2017. The redefinition of Cretaceous-Paleogene lithostratigraphic units and tectonostratigraphic division in southern Tibet. Earth Science Frontiers, 24 (1): 174-194. (in Chinese with English abstract).

Hu, X., Sinclair, H.D., Wang, J., Jiang, H. and Wu, F., 2012. Late Cretaceous ‐ Palaeogene stratigraphic and basin evolution in the Zhepure Mountain of southern Tibet: implications for the timing of India ‐ Asia initial collision. Basin Research, 24(5): 520-543.

Huang, T.-T., Xu, J.-F., Chen, J.-L., Wu, J.-b. and Zeng, Y.-C., 2017. Sedimentary record of Jurassic northward subduction of the Bangong–Nujiang Ocean: insights from detrital zircons. International Geology Review, 59(2): 166-184.

Ibañez-Mejia, M., Pullen, A., Pepper, M., Urbani, F., Ghoshal, G. and Ibañez-Mejia, J.C., 2018. Use and abuse of detrital zircon U-Pb geochronology—A case from the Río Orinoco delta, eastern Venezuela. Geology, 46(11): 1019-1022.

Jadoul, F., Berra, F. and Garzanti, E., 1998. The Tethys Himalayan passive margin from Late Triassic to Early Cretaceous (South Tibet). Journal of Asian Earth Sciences, 16(2): 173-194.

Ji, W.-Q., Wu, F.-Y., Chung, S.-L., Li, J.-X. and Liu, C.-Z., 2009. Zircon U–Pb geochronology and Hf isotopic constraints on petrogenesis of the Gangdese batholith, southern Tibet. Chemical Geology, 262(3): 229-245.

Kapp, P., DeCelles, P.G., Gehrels, G.E., Heizler, M. and Ding, L., 2007. Geological records of the Lhasa-Qiangtang and Indo-Asian collisions in the Nima area of central Tibet. GSA Bulletin, 119(7-8): 917-933.

Kapp, P., Yin, A., Harrison, T.M. and Ding, L., 2005. Cretaceous-Tertiary shortening, basin development, and volcanism in central Tibet. GSA Bulletin, 117(7-8): 865-878.

Kapp, P., Yin, A., Manning, C.E., Harrison, T.M., Taylor, M.H. and Ding, L., 2003. Tectonic evolution of the early Mesozoic blueschist-bearing Qiangtang metamorphic belt, central Tibet. Tectonics, 22(4).

Kapp, P., Yin, A., Manning, C.E., Murphy, M., Harrison, T.M., Spurlin, M., Lin, D., Xi-Guang, D. and Cun-Ming, W., 2000. Blueschist-bearing metamorphic core complexes in the Qiangtang block reveal deep crustal structure of northern Tibet. Geology, 28(1): 19-22.

Lai, W., Hu, X., Garzanti, E., Sun, G., Garzione, C.N., BouDagher Fadel, M. and Ma, A., 2019a. Initial growth of the Northern Lhasaplano, Tibetan Plateau in the early Late Cretaceous (ca. 92 Ma). GSA Bulletin, 131(11-12): 1823-1836.

Lai, W., Hu, X., Garzanti, E., Xu, Y., Ma, A. and Li, W., 2019b. Early Cretaceous sedimentary evolution of the northern Lhasa terrane and the timing of initial Lhasa-Qiangtang collision.

Gondwana Research, 73: 136-152.

Lai, W., Hu, X., Zhu, D., An, W. and Ma, A., 2017. Discovery of the early Jurassic Gajia mélange in the Bangong–Nujiang suture zone: Southward subduction of the Bangong–Nujiang Ocean? International Journal of Earth Sciences, 106(4): 1277-1288.

LaMaskin, T.A., 2012. Detrital zircon facies of Cordilleran terranes in western North America. GSA Today, 22(3): 4-11.

Laskowski, A.K., Orme, D.A., Cai, F. and Ding, L., 2019. The Ancestral Lhasa River: A Late Cretaceous trans-arc river that drained the proto–Tibetan Plateau. Geology, 47(11): 1029-1033.

Leary, R.J., DeCelles, P.G., Quade, J., Gehrels, G.E. and Waanders, G., 2016. The Liuqu Conglomerate, southern Tibet: Early Miocene basin development related to deformation within the Great Counter Thrust system. Lithosphere, 8(5): 427-450.

Lee, H.-Y., Chung, S.-L., Lo, C.-H., Ji, J., Lee, T.-Y., Qian, Q. and Zhang, Q., 2009. Eocene Neotethyan slab breakoff in southern Tibet inferred from the Linzizong volcanic record. Tectonophysics, 477(1): 20-35.

Leier, A.L., DeCelles, P.G., Kapp, P. and Gehrels, G.E., 2007. Lower Cretaceous Strata in the Lhasa Terrane, Tibet, with Implications for Understanding the Early Tectonic History of the Tibetan Plateau. Journal of Sedimentary Research, 77(10): 809-825.

Li, C., 1987. The Longmucuo-Shuanghu-Lancangjiang plate suture and the north boundary of distribution of Gondwana facies Permo-Carboniferous system in northern Xizang. China. Journal of Changchun College of Geology, 17(2): 155-166.

Li, C., Hu, X., Wang, J., Vermeesch, P. and Garzanti, E., 2020a. Sandstone provenance analysis in Longyan supports the existence of a Late Paleozoic continental arc in South China. Tectonophysics, 780: 228400.

Li, C., Wang, G.H., Zhao, Z.B., Du, J.X., Ma, X.X. and Zheng, Y.L., 2020b. Late Mesozoic tectonic evolution of the central Bangong–Nujiang Suture Zone, central Tibetan Plateau. International Geology Review, 62(18): 2300-2323.

Li, C., Wu, Y., Wang, M. and Yang, H., 2010. Significant progress on Pan-African and early Paleozoic orogenic events in Qinghai–Tibet Plateau: discovery of Pan-African orogenic unconformity and Cambrian System in the Gangdese area, Tibet, China. Geological Bulletin of China, 29(12): 1733-1736.

Li, G., Sandiford, M., Liu, X., Xu, Z., Wei, L. and Li, H., 2014a. Provenance of Late Triassic sediments in central Lhasa terrane, Tibet and its implication. Gondwana Research, 25(4): 1680-1689.

Li, G., Kohn, B., Sandiford, M., Xu, Z. and Wei, L., 2015. Constraining the age of Liuqu Conglomerate, southern Tibet: Implications for evolution of the India–Asia collision zone. Earth and Planetary Science Letter, 426(15): 259-266.

Li, G., Wan, X., Liu, W., Liang, D. and Hyesu, Y., 2005. Discovery of Paleogene marine stratum along the southern side of Yarlung-Zangbo suture zone and its implications in tectonics. Science in China Series D: Earth Sciences, 48(5): 647-661.

Li, G. B. and Wan, X.Q., 2003. Eocene microfossils in southern Tibet and the final closing of the Tibetan Tethys. Journal of Stratigraphy, 27(2): 99-108. (in Chinese with English abstract).

Li, J., Hu, X., Garzanti, E., An, W. and Wang, J., 2015. Paleogene carbonate microfacies and sandstone provenance (Gamba area, South Tibet): Stratigraphic response to initial India–Asia continental collision. Journal of Asian Earth Sciences, 104: 39-54.

Li, S.-M., Wang, Q., Zhu, D.-C., Cawood, P.A., Stern, R.J., Weinberg, R., Zhao, Z. and Mo, X.-X., 2020c. Reconciling Orogenic Drivers for the Evolution of the Bangong-Nujiang Tethys During Middle-Late Jurassic. Tectonics, 39(2): e2019TC005951.

Li, S.-M., Zhu, D.-C., Wang, Q., Zhao, Z.-D., Sui, Q.-L., Liu, S.-A., Liu, D. and Mo, X.-X., 2014b. Northward subduction of Bangong–Nujiang Tethys: Insight from Late Jurassic intrusive rocks from Bangong Tso in western Tibet. Lithos, 205: 284-297.

Li, S., Ding, L., Guilmette, C., Fu, J., Xu, Q., Yue, Y. and Henrique-Pinto, R., 2017a. The subduction-accretion history of the Bangong-Nujiang Ocean: Constraints from provenance and geochronology of the Mesozoic strata near Gaize, central Tibet. Tectonophysics, 702: 42-60.

Li, S., Guilmette, C., Ding, L., Xu, Q., Fu, J.-J. and Yue, Y.-H., 2017b. Provenance of Mesozoic clastic rocks within the Bangong-Nujiang suture zone, central Tibet: Implications for the age of the initial Lhasa-Qiangtang collision. Journal of Asian Earth Sciences, 147: 469-484.

Li, S., Yin, C., Guilmette, C., Ding, L. and Zhang, J., 2019. Birth and demise of the Bangong-Nujiang Tethyan Ocean: A review from the Gerze area of central Tibet. Earth-Science Reviews, 198: 102907.

Li, X., Mattern, F., Zhang, C., Zeng, Q. and Mao, G., 2016. Multiple sources of the Upper Triassic flysch in the eastern Himalaya Orogen, Tibet, China: Implications to palaeogeography and palaeotectonic evolution. Tectonophysics, 666: 12-22.

Li, Z., Yang, J., Xu, Z., Li, T., Xu, X., Ren, Y. and Robinson, P.T., 2009. Geochemistry and Sm–Nd and Rb–Sr isotopic composition of eclogite in the Lhasa terrane, Tibet, and its geological significance. Lithos, 109(3): 240-247.

Liang, X., Wang, G., Gao, J., Jiang, H., Yuan, G., Li, D., Cao, W., Zheng, Y., Fang, Q., Lee, B.-S., Park, S.-I., Wang, Y. and Zhao, J., 2021. A late Permian–Triassic trench-slope basin in the Central Qiangtang metamorphic belt, Northern Tibet: Stratigraphy, sedimentology, syndepositional deformation and tectonic implications. Basin Research, 33(4): 2383-2410.

Lin, X. W., 1998. Sedimentary chaotic melanges and their tectonic significance: Upper Cretaceous Zongzhuo Formation, Gyangze, Xizang. Petrographic paleogeography, 18(2): 28-33. (in Chinese with English abstract).

Liu, A.-L., Wang, Q., Zhu, D.-C., Zhao, Z.-D., Liu, S.-A., Wang, R., Dai, J.-G., Zheng, Y.-C. and Zhang, L.-L., 2018. Origin of the ca. 50 Ma Linzizong shoshonitic volcanic rocks in the eastern Gangdese arc, southern Tibet. Lithos, 304-307: 374-387.

Liu, D., Shi, R., Ding, L., Huang, Q., Zhang, X., Yue, Y. and Zhang, L., 2017. Zircon U–Pb age and Hf isotopic compositions of Mesozoic granitoids in southern Qiangtang, Tibet: Implications for the subduction of the Bangong–Nujiang Tethyan Ocean. Gondwana Research, 41: 157-172.

Liu, G. and Einsele, G., 1996. Various types of olistostromes in a closing ocean basin, Tethyan Himalaya (Cretaceous, Tibet). Sedimentary Geology, 104(1): 203-226.

Liu, J. and Aitchison, J.C., 2002. Upper Paleocene Radiolarians from the Yamdrok Mélange, South Xizang (Tibet), China. Micropaleontology, 48: 145-154.

Liu, Q., Kneller, B., An, W. and Hu, X., 2021. Sedimentological responses to initial continental collision: triggering of sand injection and onset of mass movement in a syn-collisional trench basin, Saga, southern Tibet. Journal of the Geological Society, 178(6): jgs2020-178.

Ludwing, K., 2003. Isoplot/Ex Version 3.0 A-Geochronological Toolkit for Mircrosoft Excel. Berkeley: Berkeley Geochronological Centre Special Publication.

Luo, A.-B., Fan, J.-J., Hao, Y.-J., Li, H. and Zhang, B.-C., 2020. Aptian Flysch in Central Tibet:

Constraints on the Timing of Closure of the Bangong-Nujiang Tethyan Ocean. Tectonics, 39(12): e2020TC006198.

Ma, A., Hu, X., Garzanti, E., Han, Z. and Lai, W., 2017. Sedimentary and tectonic evolution of the southern Qiangtang basin: Implications for the Lhasa-Qiangtang collision timing. Journal of Geophysical Research: Solid Earth, 122(7): 4790-4813.

Ma, A., Hu, X., Kapp, P., BouDagher-Fadel, M. and Lai, W., 2020a. Pre-Oxfordian (>163 Ma) Ophiolite Obduction in Central Tibet. Geophysical Research Letters, 47(10): e2019GL086650.

Ma, A., Hu, X., Kapp, P., Han, Z., Lai, W. and BouDagher-Fadel, M., 2018. The disappearance of a Late Jurassic remnant sea in the southern Qiangtang Block (Shamuluo Formation, Najiangco area): Implications for the tectonic uplift of central Tibet. Palaeogeography, Palaeoclimatology, Palaeoecology, 506: 30-47.

Ma, A., Hu, X., Kapp, P., Lai, W., Han, Z. and Xue, W., 2020b. Mesozoic Subduction Accretion History in Central Tibet Constrained From Provenance Analysis of the Mugagangri Subduction Complex in the Bangong-Nujiang Suture Zone. Tectonics, 39(9): e2020TC006144.

Malusà, M.G. and Fitzgerald, P.G., 2020. The geologic interpretation of the detrital thermochronology record within a stratigraphic framework, with examples from the European Alps, Taiwan and the Himalayas. Earth-Science Reviews, 201: 103074.

Malusà, M.G. and Garzanti, E., 2019. The Sedimentology of Detrital Thermochronology. In: M.G. Malusà and P.G. Fitzgerald (Editors), Fission-Track Thermochronology and its Application to Geology. Springer International Publishing, Cham, pp. 123-143.

Matthews, W., Guest, B. and Madronich, L., 2018. Latest Neoproterozoic to Cambrian detrital zircon facies of western Laurentia. Geosphere, 14(1): 243-264.

Meng, Z., Wang, J., Ji, W., Zhang, H., Wu, F. and Garzanti, E., 2019. The Langjiexue Group is an in situ sedimentary sequence rather than an exotic block: Constraints from coeval Upper Triassic strata of the Tethys Himalaya (Qulonggongba Formation). Science China Earth Sciences, 62(5): 783-797.

Mo, X., Hou, Z., Niu, Y., Dong, G., Qu, X., Zhao, Z. and Yang, Z., 2007. Mantle contributions to crustal thickening during continental collision: Evidence from Cenozoic igneous rocks in southern Tibet. Lithos, 96(1): 225-242.

Najman, Y., 2006. The detrital record of orogenesis: A review of approaches and techniques used in the Himalayan sedimentary basins. Earth-Science Reviews, 74(1): 1-72.

Orme, D.A., Carrapa, B. and Kapp, P., 2015. Sedimentology, provenance and geochronology of the upper Cretaceous–lower Eocene western Xigaze forearc basin, southern Tibet. Basin Research, 27(4): 387-411.

Orme, D.A., Laskowski, A.K., Zilinsky, M.F., Chao, W., Guo, X., Cai, F. and Lin, D., 2021. Sedimentology and provenance of newly identified Upper Cretaceous trench basin strata, Dênggar, southern Tibet: Implications for development of the Eurasian margin prior to India–Asia collision. Basin Research, 33(2): 1454-1473.

Ortega-Flores, B., Solari, L.A. and Martini, M., 2021. Multidimensional Scaling (MDS): A quantitative approximation of zircon ages to sedimentary provenance with some examples from Mexico. Journal of South American Earth Sciences, 110: 103347.

Pastore, G., Baird, T., Vermeesch, P., Bristow, C., Resentini, A. and Garzanti, E., 2021. Provenance and recycling of Sahara Desert sand. Earth-Science Reviews, 216: 103606.

Pullen, A., Ibáñez-Mejía, M., Gehrels, G.E., Ibáñez-Mejía, J.C. and Pecha, M., 2014. What happens when n= 1000? Creating large-n geochronological datasets with LA-ICP-MS for geologic investigations. Journal of Analytical Atomic Spectrometry, 29(6): 971-980.

Pullen, A. and Kapp, P., 2014. Mesozoic tectonic history and lithospheric structure of the Qiangtang terrane: Insights from the Qiangtang metamorphic belt, central Tibet. Geological Society of America Special Papers, 507: 71-87.

Pullen, A., Kapp, P., Gehrels, G.E., Ding, L. and Zhang, Q., 2011. Metamorphic rocks in central Tibet: Lateral variations and implications for crustal structure. GSA Bulletin, 123(3-4): 585-600.

Pullen, A., Kapp, P., Gehrels, G.E., Vervoort, J.D. and Ding, L., 2008. Triassic continental subduction in central Tibet and Mediterranean-style closure of the Paleo-Tethys Ocean. Geology, 36(5): 351-354.

Schwartz, T.M., Schwartz, R.K. and Weislogel, A.L., 2019. Orogenic Recycling of Detrital Zircons Characterizes Age Distributions of North American Cordilleran Strata. Tectonics, 38(12): 4320-4334.

Sciunnach, D. and Garzanti, E., 2012. Subsidence history of the Tethys Himalaya. Earth-Science Reviews, 111(1): 179-198.

Searle, M.P., Windley, B.F., Coward, M.P., Cooper, D.J.W., Rex, A.J., Rex, D., Tingdong, L., Xuchang, X., Jan, M.Q., Thakur, V.C. and Kumar, S., 1987. The closing of Tethys and the tectonics of the Himalaya. GSA Bulletin, 98(6): 678-701.

Sharman, G.R., Sharman, J.P. and Sylvester, Z., 2018. detritalPy: A Python-based toolset for visualizing and analysing detrital geo-thermochronologic data. The Depositional Record, 4(2): 202-215.

Sircombe, K.N., 2004. AgeDisplay: an EXCEL workbook to evaluate and display univariate geochronological data using binned frequency histograms and probability density distributions. Computers & Geosciences, 30(1): 21-31.

Sircombe, K.N. and Hazelton, M.L., 2004. Comparison of detrital zircon age distributions by kernel functional estimation. Sedimentary Geology, 171(1): 91-111.

Spencer, C.J., Kirkland, C.L. and Taylor, R.J.M., 2016. Strategies towards statistically robust interpretations of in situ U–Pb zircon geochronology. Geoscience Frontiers, 7(4): 581-589.

Sun, G. Y., Hu, X. M. and Wang, J. G., 2011. Petrologic and provenance analysis of the Zongzhuo melange in Baihe area, Gyangze, southern Tibet. Acta Geologica Sinica, 85(8): 1343-1351. (in Chinese with English abstract).

Sun, G., Hu, X. and Sinclair, H.D., 2017. Early Cretaceous palaeogeographic evolution of the Coqen Basin in the Lhasa Terrane, southern Tibetan Plateau. Palaeogeography, Palaeoclimatology, Palaeoecology, 485: 101-118.

Sun, G., Hu, X., Xu, Y. and BouDagher-Fadel, M.K., 2019. Discovery of Middle Jurassic trench deposits in the Bangong-Nujiang suture zone: Implications for the timing of Lhasa-Qiangtang initial collision. Tectonophysics, 750: 344-358.

Sundell, K.E. and Saylor, J.E., 2021. Two-Dimensional Quantitative Comparison of Density Distributions in Detrital Geochronology and Geochemistry. Geochemistry, Geophysics, Geosystems, 22(4): e2020GC009559.

Tao, J., 1988. Plant fossils from the Liuqu Formation in Lhaze County, Xizang and their paleoclimatological significances. Memoirs of the Institute of Geology, Chinese Academy of Science. Science Press, Beijing: 223-238.

Tapponnier, P., Mercier, J., Proust, F., Andrieux, J., Armijo, R., Bassoullet, J., Brunel, M., Burg, J., Colchen, M. and Dupre, B., 1981. The Tibetan side of the India–Eurasia collision. Nature, 294(5840): 405-410.

Taylor, S.R. and McLennan, S.M., 1995. The geochemical evolution of the continental crust. Reviews of Geophysics, 33(2): 241-265.

Vermeesch, P., 2012. On the visualisation of detrital age distributions. Chemical Geology, 312: 190-194.

Vermeesch, P., 2013. Multi-sample comparison of detrital age distributions. Chemical Geology, 341: 140-146.

Vermeesch, P. and Garzanti, E., 2015. Making geological sense of 'Big Data' in sedimentary provenance analysis. Chemical Geology, 409: 20-27.

Wan, X., Wang, L., Wang, C. and Jansa, L., 1998. Discovery and significance of Cretaceous fossils from the Xigaze Forearc Basin, Tibet. Journal of Asian Earth Sciences, 16(2): 217-223.

Wang, B.-D., Wang, L.-Q., Chung, S.-L., Chen, J.-L., Yin, F.-G., Liu, H., Li, X.-B. and Chen, L.-K., 2016a. Evolution of the Bangong–Nujiang Tethyan ocean: Insights from the geochronology and geochemistry of mafic rocks within ophiolites. Lithos, 245: 18-33.

Wang, J.-G., Hu, X.-M., Wu, F.-Y. and Jansa, L., 2010. Provenance of the Liuqu Conglomerate in southern Tibet: A Paleogene erosional record of the Himalayan–Tibetan orogen. Sedimentary Geology, 231(3): 74-84.

Wang, J.-G., Hu, X., Garzanti, E., An, W. and Liu, X.-C., 2017. The birth of the Xigaze forearc basin in southern Tibet. Earth and Planetary Science Letters, 465: 38-47.

Wang, J.-G., Hu, X., Garzanti, E., BouDagher-Fadel, M.K., Liu, Z.-C., Li, J. and Wu, F.-Y., 2020. From extension to tectonic inversion: Mid-Cretaceous onset of Andean-type orogeny in the Lhasa block and early topographic growth of Tibet. GSA Bulletin, 132(11-12): 2432-2454.

Wang, J.-G., Wu, F.-Y., Garzanti, E., Hu, X., Ji, W.-Q., Liu, Z.-C. and Liu, X.-C., 2016b. Upper Triassic turbidites of the northern Tethyan Himalaya (Langjiexue Group): The terminal of a sediment-routing system sourced in the Gondwanide Orogen. Gondwana Research, 34: 84-98.

Wang, Q., Zhu, D.-C., Cawood, P.A., Chung, S.-L. and Zhao, Z.-D., 2021a. Resolving the Paleogeographic Puzzle of the Lhasa Terrane in Southern Tibet. Geophysical Research Letters, 48(15): e2021GL094236.

Wang, T., Li, G. and Elmes, M., 2021b. Biostratigraphy and provenance analysis of the Cretaceous to Palaeogene deposits in southern Tibet: Implications for the India-Asia collision. Basin Research, 33(3): 1749-1775.

Wang, Z., Yu, F., Wang, J., Fu, X., Chen, W., Zeng, S. and Song, C., 2021c. Palaeoenvironment evolution and organic matter accumulation of the Upper Triassic mudstones from the eastern Qiangtang Basin (Tibet), eastern Tethys. Marine and Petroleum Geology, 130: 105113.

Wei, L., Liu, X., Yan, F., Mai, X., Zhou, X., Li, G. and Liu, X., 2009. Discovery and preliminary study on palynofossils from the Paleogene Liuqu Conglomerates in southern Xizang (Tibet). Acta Microbiol Sin, 26(3): 249-260.

Wen, D.-R., Liu, D., Chung, S.-L., Chu, M.-F., Ji, J., Zhang, Q., Song, B., Lee, T.-Y., Yeh, M.-W. and Lo, C.-H., 2008. Zircon SHRIMP U–Pb ages of the Gangdese Batholith and implications for Neotethyan subduction in southern Tibet. Chemical Geology, 252(3): 191-201.

Willems, H., Zhou, Z., Zhang, B. and Gräfe, K.U., 1996. Stratigraphy of the upper cretaceous and lower tertiary strata in the Tethyan Himalayas of Tibet (Tingri area, China). Geologische

Rundschau, 85(4): 723.

Wu, F.-Y., Ji, W.-Q., Liu, C.-Z. and Chung, S.-L., 2010. Detrital zircon U–Pb and Hf isotopic data from the Xigaze fore-arc basin: Constraints on Transhimalayan magmatic evolution in southern Tibet. Chemical Geology, 271(1): 13-25.

Wu, H. R., Wang, D. A. and Wang, L. C., 1977. The Cretaceous of Laze-Jiangze district, southern Xizang. Scientia Geologica Sinca, 3: 250-262. (in Chinese with English abstract).

Xu, Y., Hu, X., Garzanti, E., BouDagher-Fadel, M., Sun, G., Lai, W. and Zhang, S., 2021. Mid-Cretaceous thick carbonate accumulation in Northern Lhasa (Tibet): eustatic vs. tectonic control? GSA Bulletin, 134(1-2): 389-404.

Xue, W., Hu, X., Ma, A., Garzanti, E. and Li, J., 2020. Eustatic and tectonic control on the evolution of the Jurassic North Qiangtang Basin, northern Tibet, China: Impact on the petroleum system. Marine and Petroleum Geology, 120: 104558.

Yan, M., Zhang, D., Fang, X., Ren, H., Zhang, W., Zan, J., Song, C. and Zhang, T., 2016. Paleomagnetic data bearing on the Mesozoic deformation of the Qiangtang Block: Implications for the evolution of the Paleo- and Meso-Tethys. Gondwana Research, 39: 292-316.

Yang, J., Xu, Z., Li, Z., Xu, X., Li, T., Ren, Y., Li, H., Chen, S. and Robinson, P.T., 2009. Discovery of an eclogite belt in the Lhasa block, Tibet: A new border for Paleo-Tethys? Journal of Asian Earth Sciences, 34(1): 76-89.

Yu, G. M., Zhang, S. N. and Wang, C. S., 1990. Geogocial interpretation on the results of cluster analysis of trace elements from argillaceous rocks in the Jurassic, Cretaceous and Tertiary strata in Xizang. 5: 1-7. (in Chinese with English abstract).

Zeng, M., Zhang, X., Cao, H., Ettensohn, F.R., Cheng, W. and Lang, X., 2016. Late Triassic initial subduction of the Bangong - Nujiang Ocean beneath Qiangtang revealed: stratigraphic and geochronological evidence from Gaize, Tibet. Basin Research, 28(1): 147-157.

Zhai, Q.-g., Jahn, B.-m., Wang, J., Hu, P.-y., Chung, S.-l., Lee, H.-y., Tang, S.-h. and Tang, Y., 2016. Oldest Paleo-Tethyan ophiolitic mélange in the Tibetan Plateau. GSA Bulletin, 128(3-4): 355-373.

Zhai, Q.-G., Zhang, R.-Y., Jahn, B.-M., Li, C., Song, S.-G. and Wang, J., 2011. Triassic eclogites from central Qiangtang, northern Tibet, China: Petrology, geochronology and metamorphic P–T path. Lithos, 125(1): 173-189.

Zhang, J., Li, Y., Zhang, H., Zhao, X., Liu, K. and Shang, Q., 2021. Provenance of Middle Jurassic sequences in the Northern Qiangtang: implications for Mesozoic exhumation of the Central Tibetan Mountain Range. International Geology Review, 63(16): 1969-1989.

Zhang, K.-J., Xia, B., Zhang, Y.-X., Liu, W.-L., Zeng, L., Li, J.-F. and Xu, L.-F., 2014. Central Tibetan Meso-Tethyan oceanic plateau. Lithos, 210-211: 278-288.

Zhang, K.-J., Zhang, Y.-X., Li, B., Zhu, Y.-T. and Wei, R.-Z., 2006. The blueschist-bearing Qiangtang metamorphic belt (northern Tibet, China) as an in situ suture zone: Evidence from geochemical comparison with the Jinsa suture. Geology, 34(6): 493-496.

Zhang, K. and Tang, X., 2009. Eclogites in the interior of the Tibetan Plateau and their geodynamic implications. Chinese Science Bulletin, 54(15): 2556.

Zhang, K., Zhang, Y., Tang, X. and Xia, B., 2012. Late Mesozoic tectonic evolution and growth of the Tibetan plateau prior to the Indo-Asian collision. Earth-Science Reviews, 114(3): 236-249.

Zhou, B., Hu, X. M., An, W., Ma, A. L. and Lai, W., 2018. Trench Deposition during the intial Indian-Asian collision: petrologic and provenance analysis of the Zongzhuo Formation,

southeastern Tibet. Acta Geologica Sinica, 92(1): 1-14. (in Chinese with English abstract).
Zhu, D.-C., Zhao, Z.-D., Niu, Y., Dilek, Y., Hou, Z.-Q. and Mo, X.-X., 2013. The origin and pre-Cenozoic evolution of the Tibetan Plateau. Gondwana Research, 23(4): 1429-1454.
Zhu, D.-C., Zhao, Z.-D., Niu, Y., Dilek, Y. and Mo, X.-X., 2011. Lhasa terrane in southern Tibet came from Australia. Geology, 39(8): 727-730.

Figure captions

Fig.1. Tectonic framework of the Tibetan Plateau (after Zhu et al., 2013), showing major tectonic subdivisions, suture zones and locations of sampled sites for detrital-zircon analysis. LSSZ = Longmu Tso-Shuanghu Suture Zone; BNZ = Bangong-Nujiang Suture Zone; SNMZ = Shiquan River-Nam Tso Mélange Zone; LMF = Luobadui-Milashan Fault; IYSZ = Indus-Yarlung Zangbo Suture Zone; STDZ = South Tibetan detachment; MCT = Main Central Thrust.

Fig.2. Geological map of the Bangong-Nujiang (a) and the Indus-Yarlung Zangbo (b) suture zones (after Li et al., 2020c and Hu et al., 2017, respectively).

Fig.3. Stratigraphic chart of South Qiangtang, North Lhasa, and Bangong-Nujiang suture zone (only units sampled for detrital-zircon analysis are shown).

Fig.4. Stratigraphic chart of South Lhasa, Tethys Himalaya and Indus-Yarlung Zangbo suture zone (only the stratigraphic units sampled for detrital-zircon analysis are shown).

Fig.5. Description of the detrital zircon database including the Reference, Sample and Grain-age information.

Fig.6. Number of grains analysed for each of the 527 samples considered in our compilation.

Fig.7. Detrital zircon age facies (DZF) of North Lhasa and South Qiangtang identified by multidimensional scaling (MDS) and kernel density estimation (KDE) plots. (a) Nonmetric MDS plot of age spectra of South Qiangtang and North Lhasa units older than the Qiangtang-Lhasa collision define five DZF (SQ-1, SQ-2; NL-1, NL-2, NL-3). (b) KDE plot of each identified DZF.

Fig.8. Detrital zircon age facies (DZF) of South Lhasa and Tethys Himalaya identified by multidimensional scaling (MDS) and kernel density estimation (KDE) plots. (a) Nonmetric MDS plot of age spectra of South Lhasa and Tethys Himalayan units older than the India-Asian collision define six DFZ (SL-1, SL-2, SL-3; TH-1, TH-2, TH-3). (b) KDE plot of each identified DZF.

Fig.9. MDS maps of detrital-zircon age spectra from sedimentary units in the Bangong-Nujiang suture zone compared to DFZ of South Qiangtang and North Lhasa.

Fig.10. MDS maps of detrital-zircon age spectra from sedimentary units in the Indus-Yarlung Zangbo suture zone compared to DFZ of South Lhasa and Tethys Himalaya.

Fig.11. a) KDE plot of U-Pb detrital-zircon ages from the Wuga Formation of the Bangong-Nujiang suture zone compared to averaged KDE curves for the entire South Qiangtang and North Lhasa; b). KDE plots of the five DFZ identified for South Qiangtang and North Lhasa.

Fig.12. a) KDE plots of U-Pb detrital-zircon ages from the Rongmawa Formation of the Indus-Yarlung Zangbo suture zone compared to averaged KDE curves for the entire South Lhasa and Tethys Himalaya; b) KDE plots of the six DFZ identified for South Lhasa and Tethys Himalaya.

Fig.13. MDS maps of detrital zircon-age spectra from the Duba (a, b) and Duoni (c, d) formations compared to the five DZF identified for South Qiangtang and North Lhasa (left panels); right panels show age distributions (legend in pie diagram).

Table 1. Detrital zircon age facies of South Qiangtang and North Lhasa.

Table 2. Detrital zircon age facies of South Lhasa and Tethys Himalaya.

Supplementary Data

Table S1 Detrital zircon database of Tibetan Plateau contains 49111 ages and 533 samples

Table S2 Original data of the MDS/KDS plots mentioned in this paper

Figure

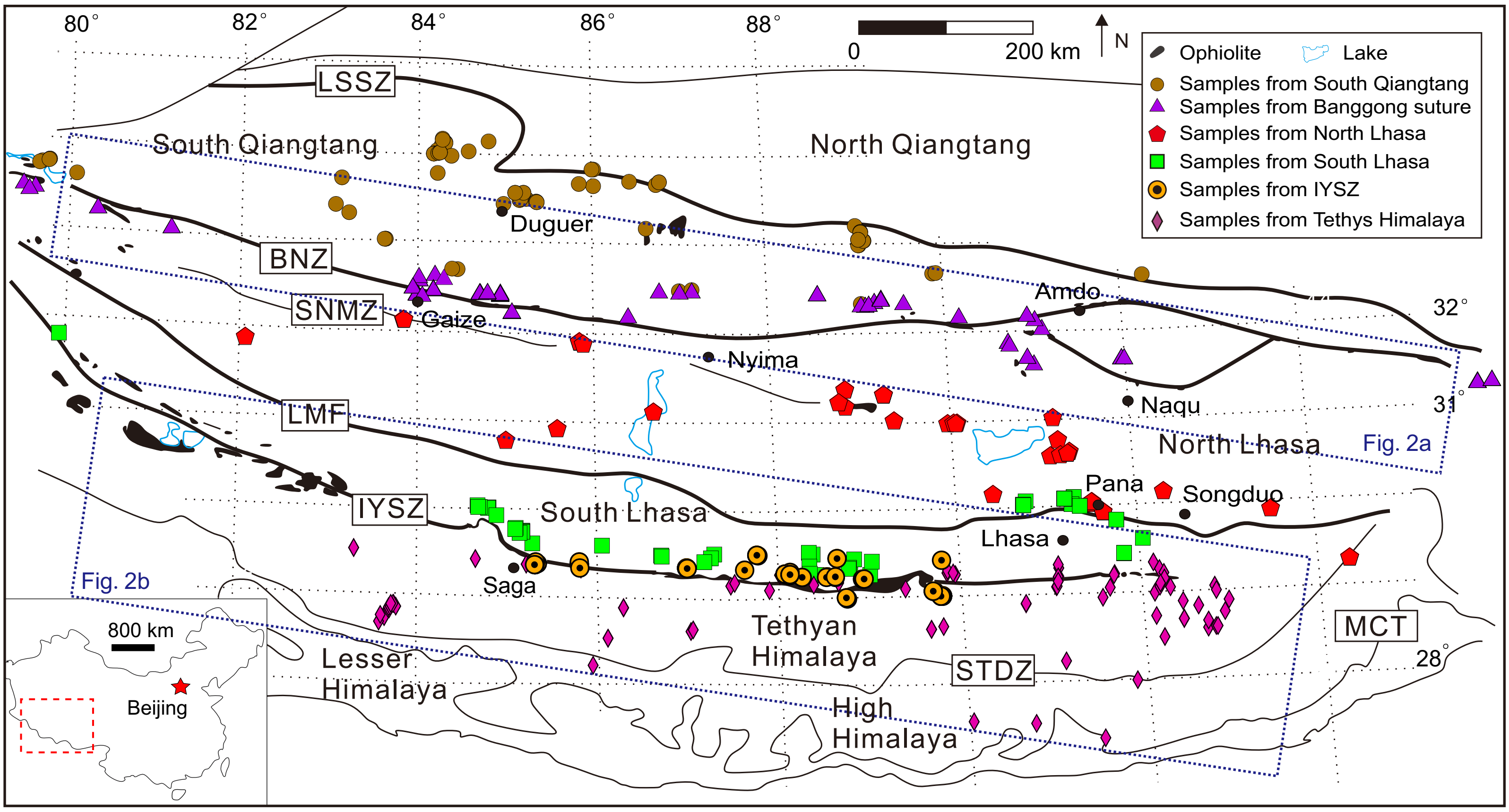

80°
82°
84°
86°
88°
0
200 km
N
Ophiolite
Lake
Samples from South Qiangtang
Samples from Banggong suture
Samples from North Lhasa
Samples from South Lhasa
Samples from IYSZ
Samples from Tethys Himalaya
LSSZ
South Qiangtang
North Qiangtang
Duguer
BNZ
SNMZ
Gaize
Amdo
32°
Nyima
Naqu
31°
LMF
North Lhasa
Fig. 2a
Pana
Songduo
IYSZ
South Lhasa
Lhasa
Saga
Fig. 2b
800 km
Beijing
Tethyan
Himalaya
MCT
28°
Lesser
Himalaya
STDZ
High
Himalaya

Fig.1

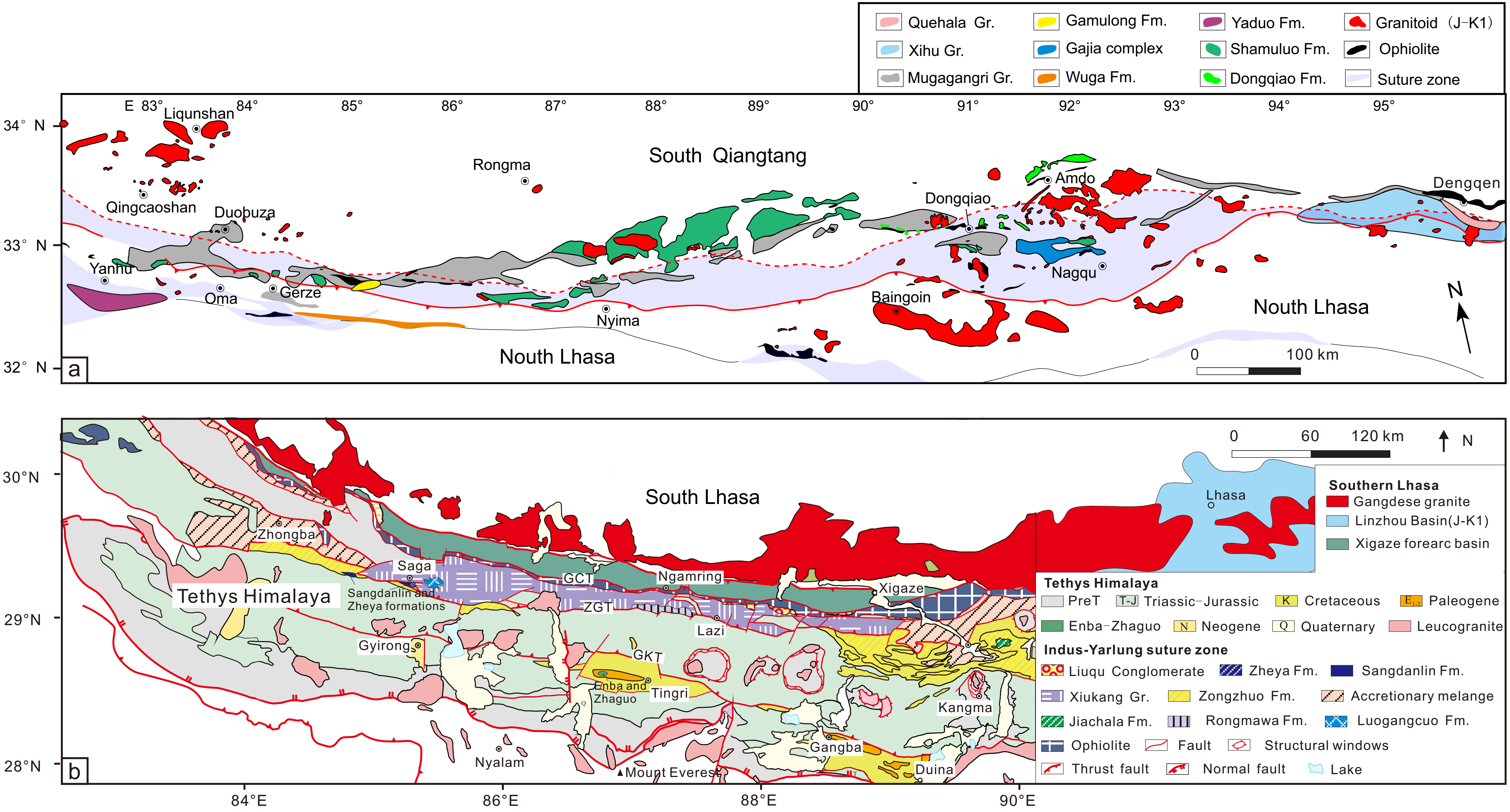

Quehala Gr.
Xihu Gr.
Mugagangri Gr.
Gamulong Fm.
Gajia complex
Wuga Fm.
Yaduo Fm.
Shamuluo Fm.
Dongqiao Fm.
Granitoid（J-K1）
Ophiolite
Suture zone
South Qiangtang
Nouth Lhasa
a
Southern Lhasa
Gangdese granite
Linzhou Basin(J-K1)
Xigaze forearc basin
Tethys Himalaya
PreT
Triassic-Jurassic
Cretaceous
Paleogene
Enba-Zhaguo
Neogene
Quaternary
Leucogranite
Indus-Yarlung suture zone
Liuqu Conglomerate
Zheya Fm.
Sangdanlin Fm.
Xiukang Gr.
Zongzhuo Fm.
Accretionary melange
Jiachala Fm.
Rongmawa Fm.
Luogangcuo Fm.
Ophiolite
Fault
Structural windows
Thrust fault
Normal fault
Lake
South Lhasa
b

Fig.2

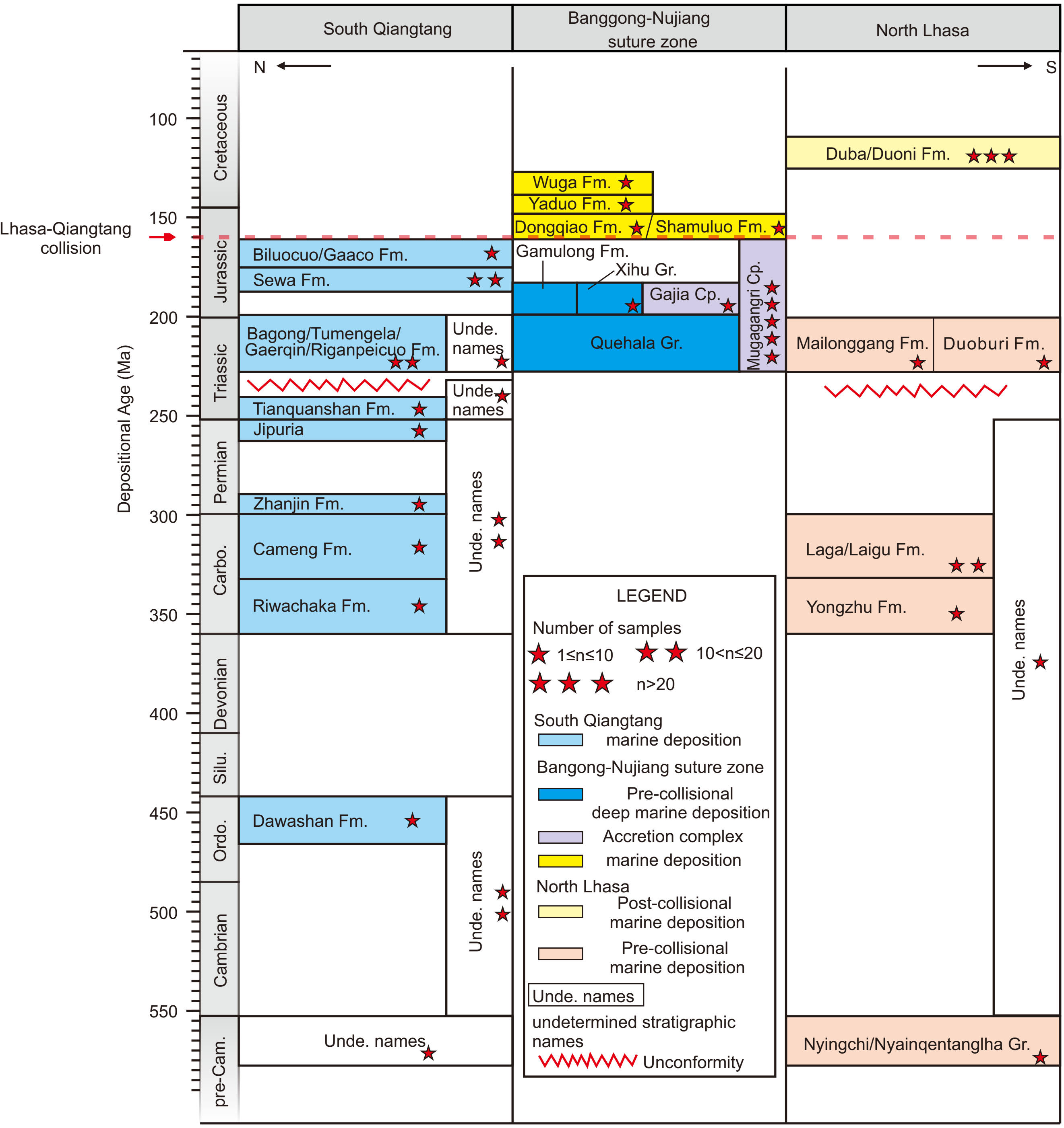
South Qiangtang
Banggong-Nujiang suture zone
North Lhasa
N
S
Depositional Age (Ma)
100
150
200
250
300
350
400
450
500
550
Cretaceous
Jurassic
Triassic
Permian
Carbo.
Devonian
Silu.
Ordo.
Cambrian
pre-Cam.
Lhasa-Qiangtang collision
Biluocuo/Gaaco Fm.
Sewa Fm.
Bagong/Tumengela/ Gaerqin/Riganpeicuo Fm.
Unde. names
Tianquanshan Fm.
Jipuria
Zhanjin Fm.
Cameng Fm.
Riwachaka Fm.
Dawashan Fm.
Unde. names
Wuga Fm.
Yaduo Fm.
Dongqiao Fm.
Shamuluo Fm.
Gamulong Fm.
Xihu Gr.
Gajia Cp.
Quehala Gr.
Mugagangri Cp.
Duba/Duoni Fm.
Mailonggang Fm.
Duoburi Fm.
Laga/Laigu Fm.
Yongzhu Fm.
Nyingchi/Nyainqentanglha Gr.
LEGEND
Number of samples
1≤n≤10
10<n≤20
n>20
South Qiangtang
marine deposition
Bangong-Nujiang suture zone
Pre-collisional deep marine deposition
Accretion complex
marine deposition
North Lhasa
Post-collisional marine deposition
Pre-collisional marine deposition
Unde. names
undetermined stratigraphic names
Unconformity

Fig.3

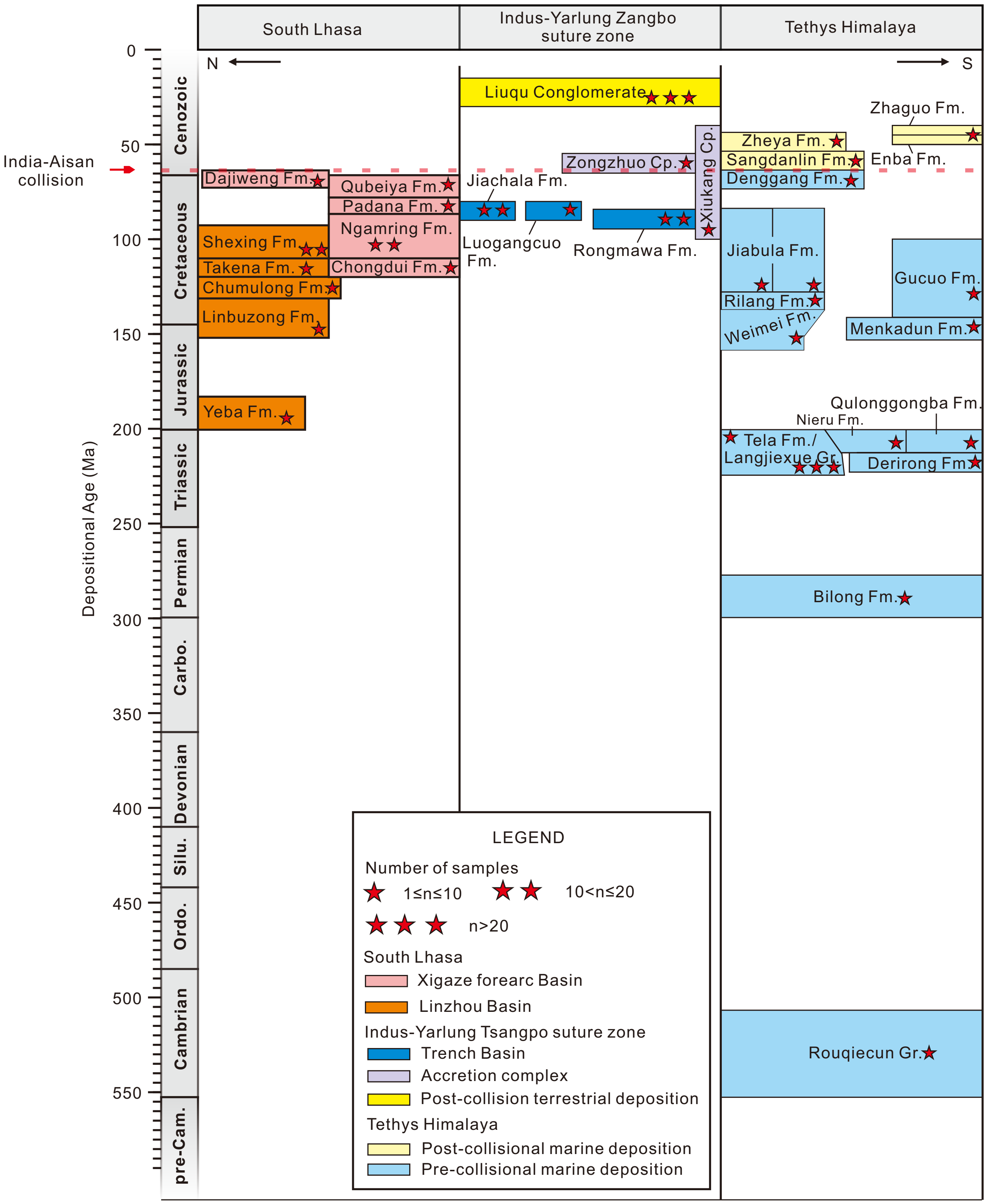
South Lhasa
Indus-Yarlung Zangbo suture zone
Tethys Himalaya
N
S
India-Aisan collision
Depositional Age (Ma)
0
50
100
150
200
250
300
350
400
450
500
550
Cenozoic
Cretaceous
Jurassic
Triassic
Permian
Carbo.
Devonian
Silu.
Ordo.
Cambrian
pre-Cam.
Dajiweng Fm.
Qubeiya Fm.
Padana Fm.
Ngamring Fm.
Chongdui Fm.
Shexing Fm.
Takena Fm.
Chumulong Fm.
Linbuzong Fm.
Yeba Fm.
Liuqu Conglomerate
Zongzhuo Cp.
Xiukang Cp.
Jiachala Fm.
Luogangcuo Fm.
Rongmawa Fm.
Zhaguo Fm.
Zheya Fm.
Sangdanlin Fm.
Enba Fm.
Denggang Fm.
Jiabula Fm.
Gucuo Fm.
Rilang Fm.
Weimei Fm.
Menkadun Fm.
Qulonggongba Fm.
Nieru Fm.
Tela Fm./ Langjiexue Gr.
Derirong Fm.
Bilong Fm.
Rouqiecun Gr.
LEGEND
Number of samples
1≤n≤10
10<n≤20
n>20
South Lhasa
Xigaze forearc Basin
Linzhou Basin
Indus-Yarlung Tsangpo suture zone
Trench Basin
Accretion complex
Post-collision terrestrial deposition
Tethys Himalaya
Post-collisional marine deposition
Pre-collisional marine deposition

Fig.4

Reference	Sample
ReferenceNumber	Unique Sample No.
Author	Published Sample_ID
Year	Region/Province
Journal	Major Geographic-Geologic Unit
Vol	Minor Geologic-Geographic Unit
Pages	Latitude
Title	Longitude
Web Link	Depos. Age

Grain age	
Sample&Grain	Published 207Pb/235U age (Ma)
206Pb/238U isotope ratio	Published 207Pb/235U 1σ uncert
206Pb/238U uncertainty (±1σ)	Published 207Pb/206Pb age (Ma)
207Pb/235U isotope ratio	Published 207Pb/206Pb 1σ uncert
207Pb/235U uncertainty (±1σ)	Best Age（Ma）
207Pb/206Pb isotope ratio	Best age uncertainty (±1σ)
207Pb/206Pb uncertainty (±1σ)	Discord ratio
Published 206Pb/238U age (Ma)	U/Th
Published 206Pb/238U 1σ uncert	Th/U

Fig.5

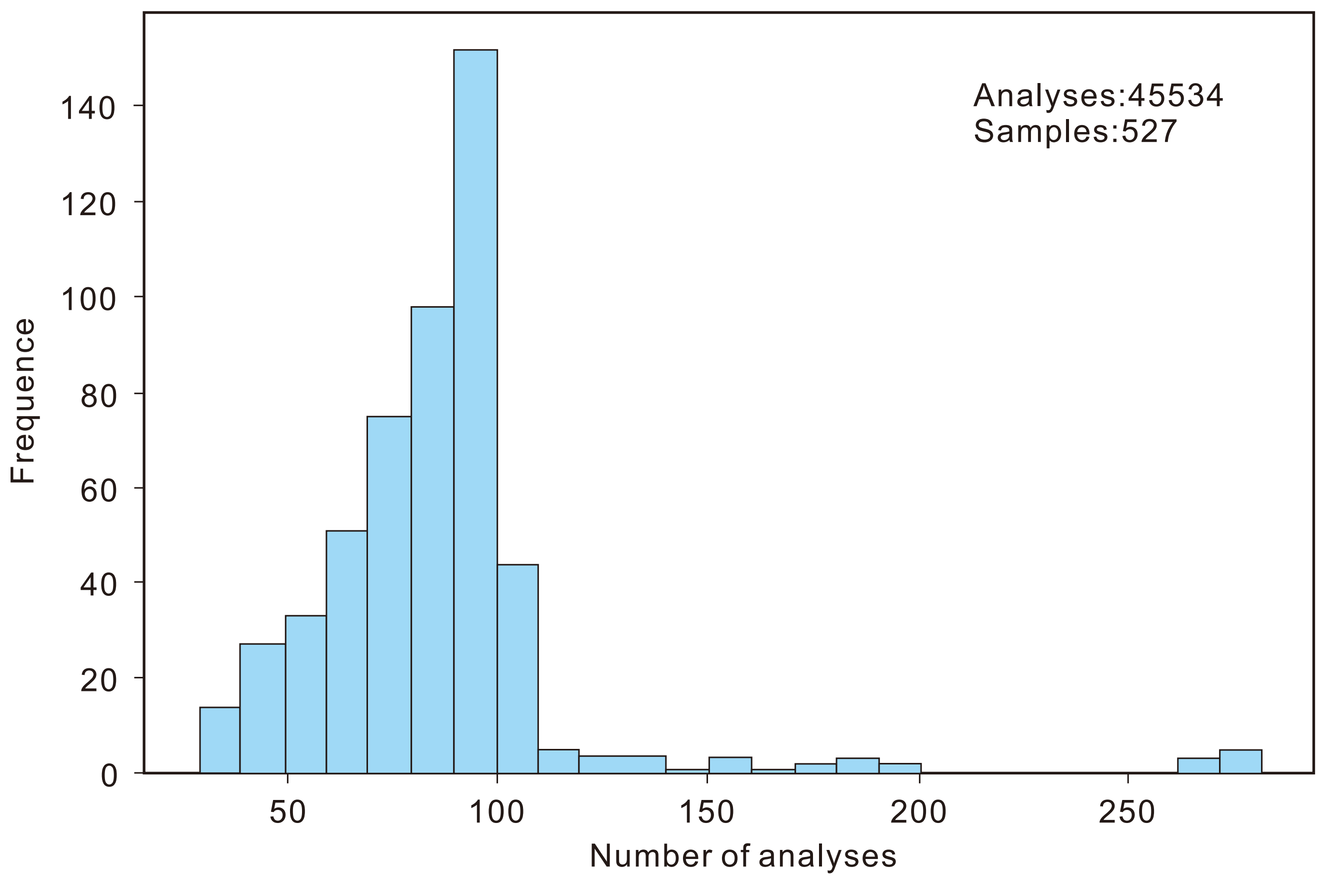

Analyses:45534
Samples:527
Frequence
0
20
40
60
80
100
120
140
50
100
150
200
250
Number of analyses

Fig.6

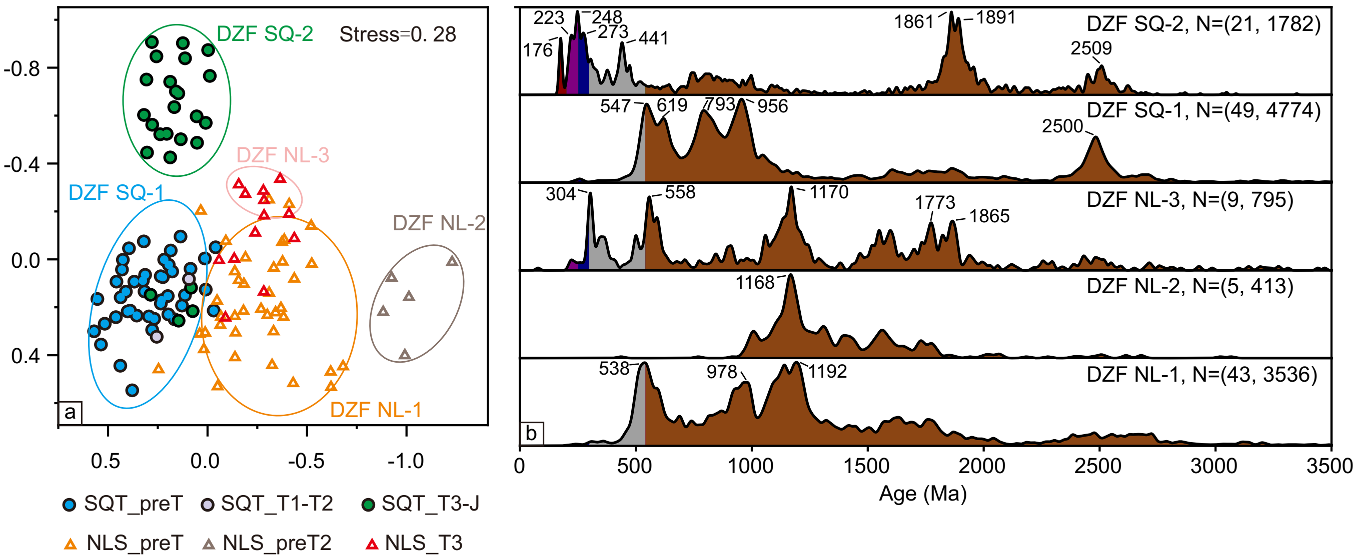

DZF SQ-2
Stress=0. 28
-0.8
-0.4
0.0
0.4
DZF NL-3
DZF SQ-1
DZF NL-2
DZF NL-1
a
0.5
0.0
-0.5
-1.0
SQT_preT
SQT_T1-T2
SQT_T3-J
NLS_preT
NLS_preT2
NLS_T3
b
DZF SQ-2, N=(21, 1782)
DZF SQ-1, N=(49, 4774)
DZF NL-3, N=(9, 795)
DZF NL-2, N=(5, 413)
DZF NL-1, N=(43, 3536)
176
223
248
273
441
1861
1891
2509
547
619
793
956
2500
304
558
1170
1773
1865
1168
538
978
1192
0
500
1000
1500
2000
2500
3000
3500
Age (Ma)

Fig.7

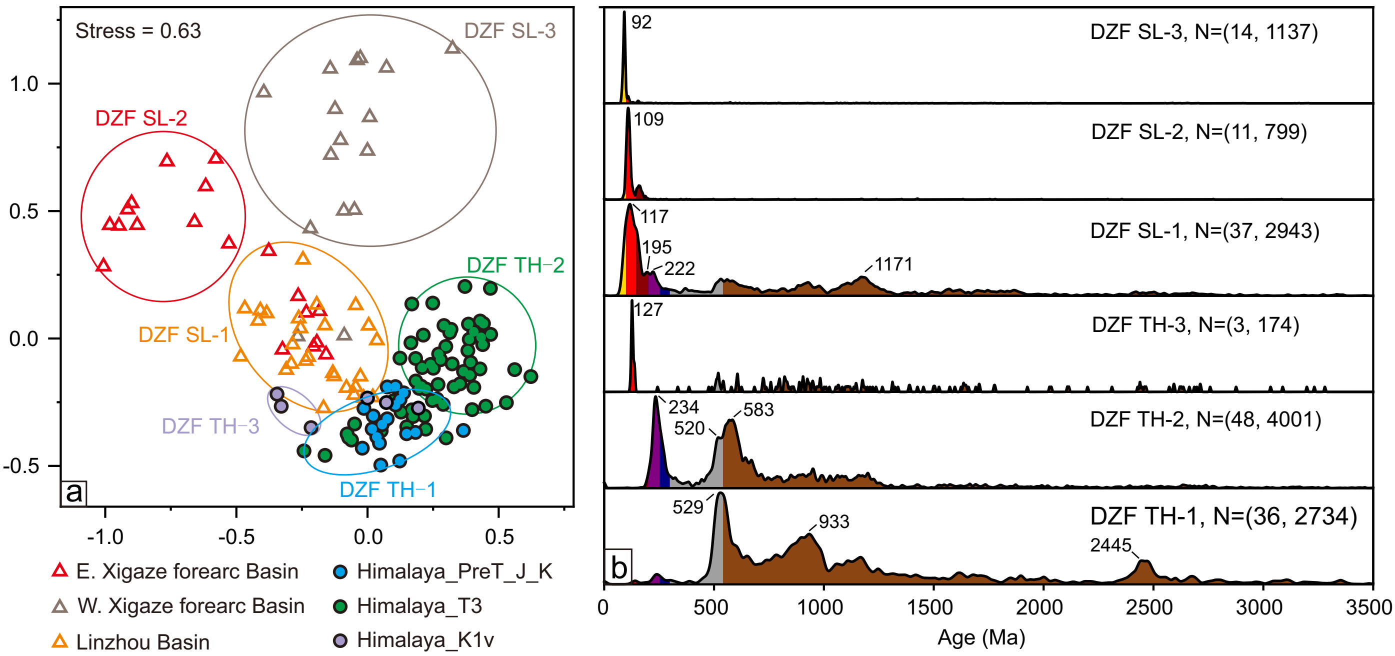

Stress = 0.63
DZF SL-3
DZF SL-2
DZF SL-1
DZF TH-2
DZF TH-3
DZF TH-1
a
E. Xigaze forearc Basin
W. Xigaze forearc Basin
Linzhou Basin
Himalaya_PreT_J_K
Himalaya_T3
Himalaya_K1v
b
DZF SL-3, N=(14, 1137)
DZF SL-2, N=(11, 799)
DZF SL-1, N=(37, 2943)
DZF TH-3, N=(3, 174)
DZF TH-2, N=(48, 4001)
DZF TH-1, N=(36, 2734)
Age (Ma)

Fig.8

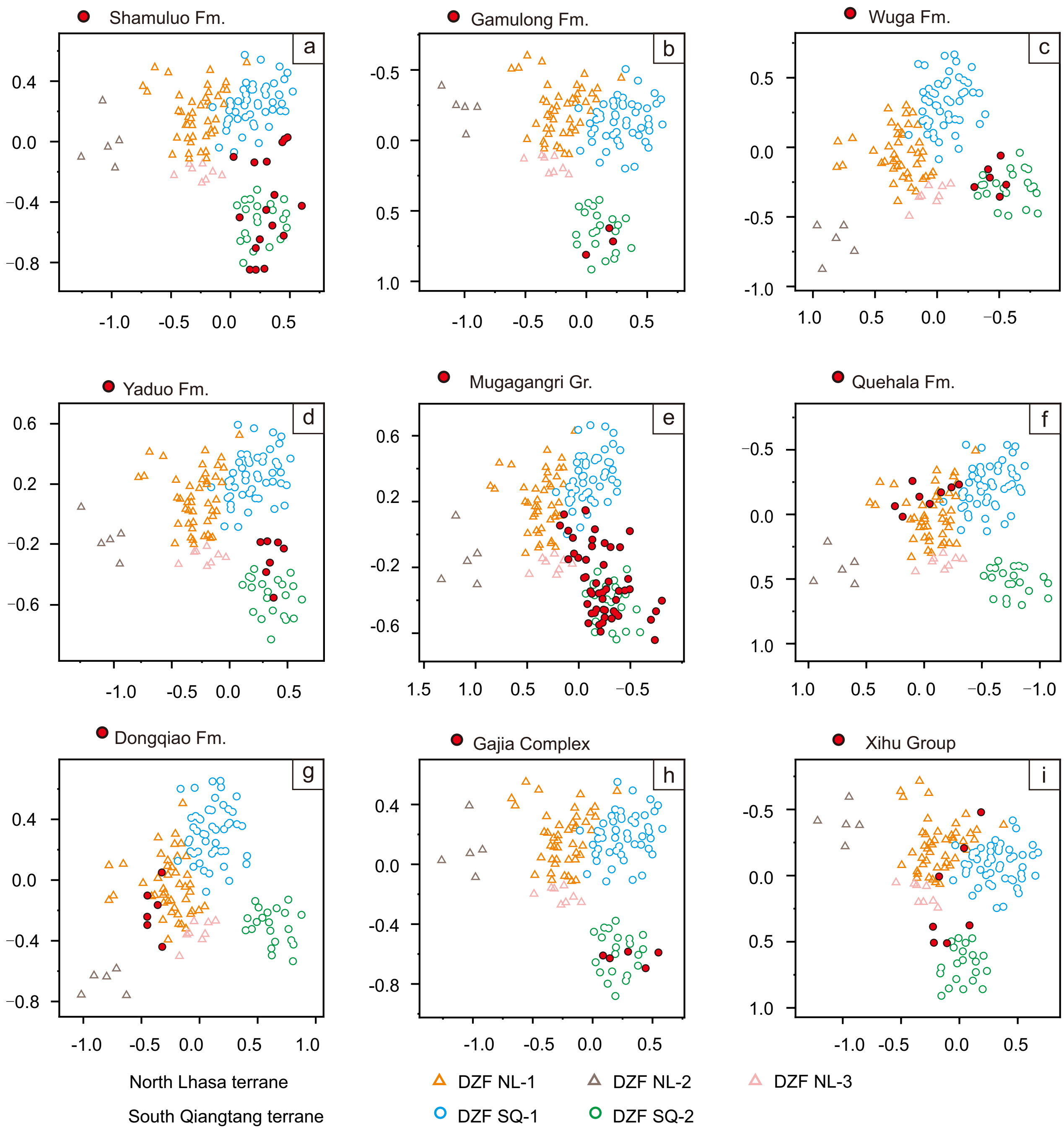
Shamuluo Fm.
Gamulong Fm.
Wuga Fm.
Yaduo Fm.
Mugagangri Gr.
Quehala Fm.
Dongqiao Fm.
Gajia Complex
Xihu Group
a
b
c
d
e
f
g
h
i
North Lhasa terrane
South Qiangtang terrane
DZF NL-1
DZF NL-2
DZF NL-3
DZF SQ-1
DZF SQ-2

Fig.9

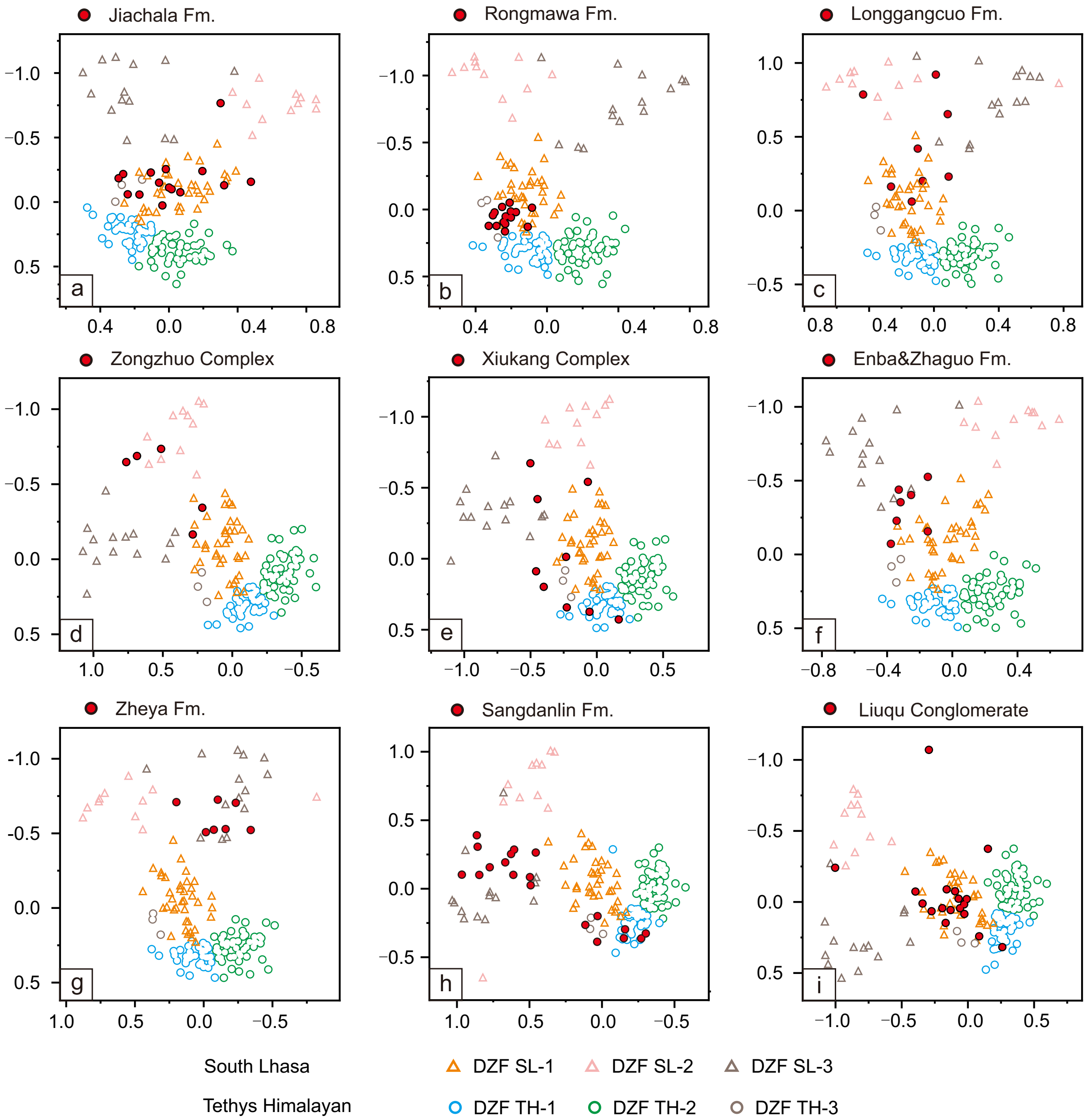

Jiachala Fm.
Rongmawa Fm.
Longgangcuo Fm.
Zongzhuo Complex
Xiukang Complex
Enba&Zhaguo Fm.
Zheya Fm.
Sangdanlin Fm.
Liuqu Conglomerate
a
b
c
d
e
f
g
h
i
South Lhasa
Tethys Himalayan
DZF SL-1
DZF SL-2
DZF SL-3
DZF TH-1
DZF TH-2
DZF TH-3

Fig.10

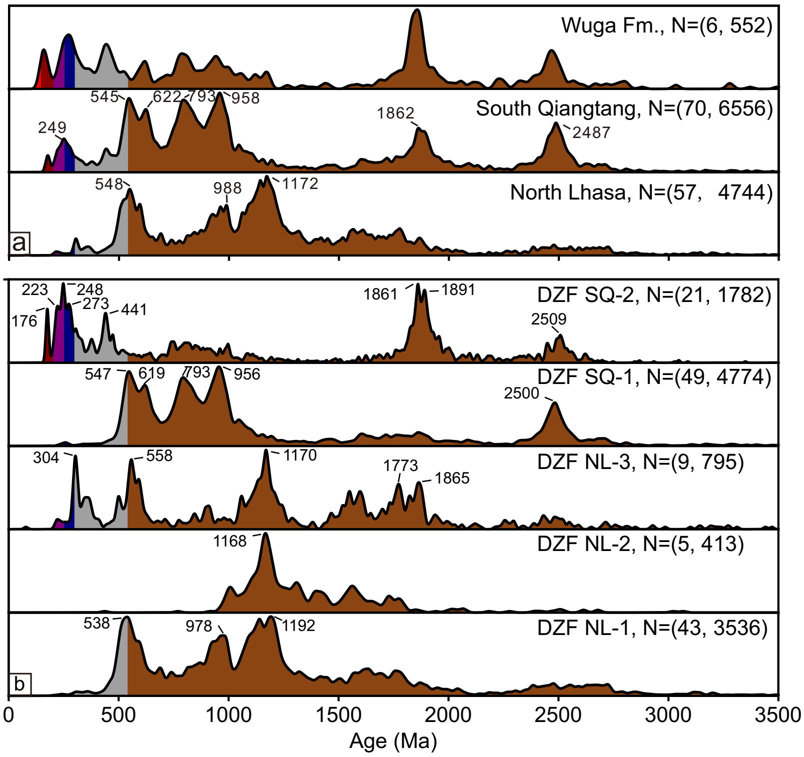
Wuga Fm., N=(6, 552)
South Qiangtang, N=(70, 6556)
249
545
622
793
958
1862
2487
North Lhasa, N=(57, 4744)
548
988
1172
a
DZF SQ-2, N=(21, 1782)
223
248
273
176
441
1861
1891
2509
DZF SQ-1, N=(49, 4774)
547
619
793
956
2500
DZF NL-3, N=(9, 795)
304
558
1170
1773
1865
DZF NL-2, N=(5, 413)
1168
DZF NL-1, N=(43, 3536)
538
978
1192
b
0
500
1000
1500
2000
2500
3000
3500
Age (Ma)

Fig.11

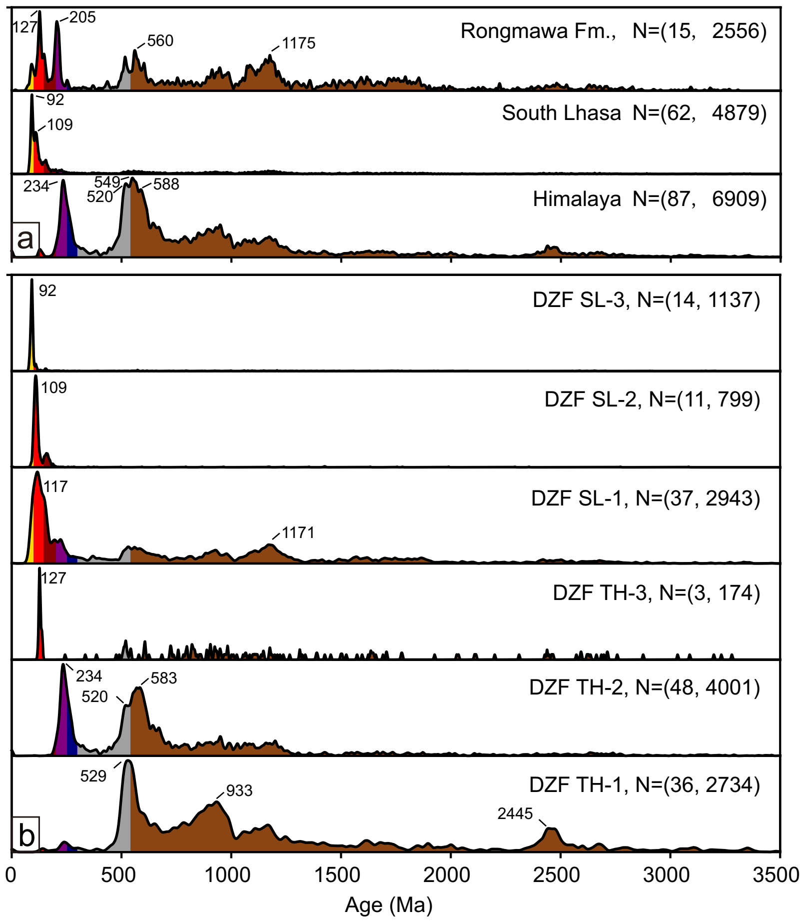
Rongmawa Fm., N=(15, 2556)
127
205
560
1175
South Lhasa N=(62, 4879)
92
109
Himalaya N=(87, 6909)
234
549
520
588
a
DZF SL-3, N=(14, 1137)
92
DZF SL-2, N=(11, 799)
109
DZF SL-1, N=(37, 2943)
117
1171
DZF TH-3, N=(3, 174)
127
DZF TH-2, N=(48, 4001)
234
520
583
DZF TH-1, N=(36, 2734)
529
933
2445
b
0
500
1000
1500
2000
2500
3000
3500
Age (Ma)

Fig.12

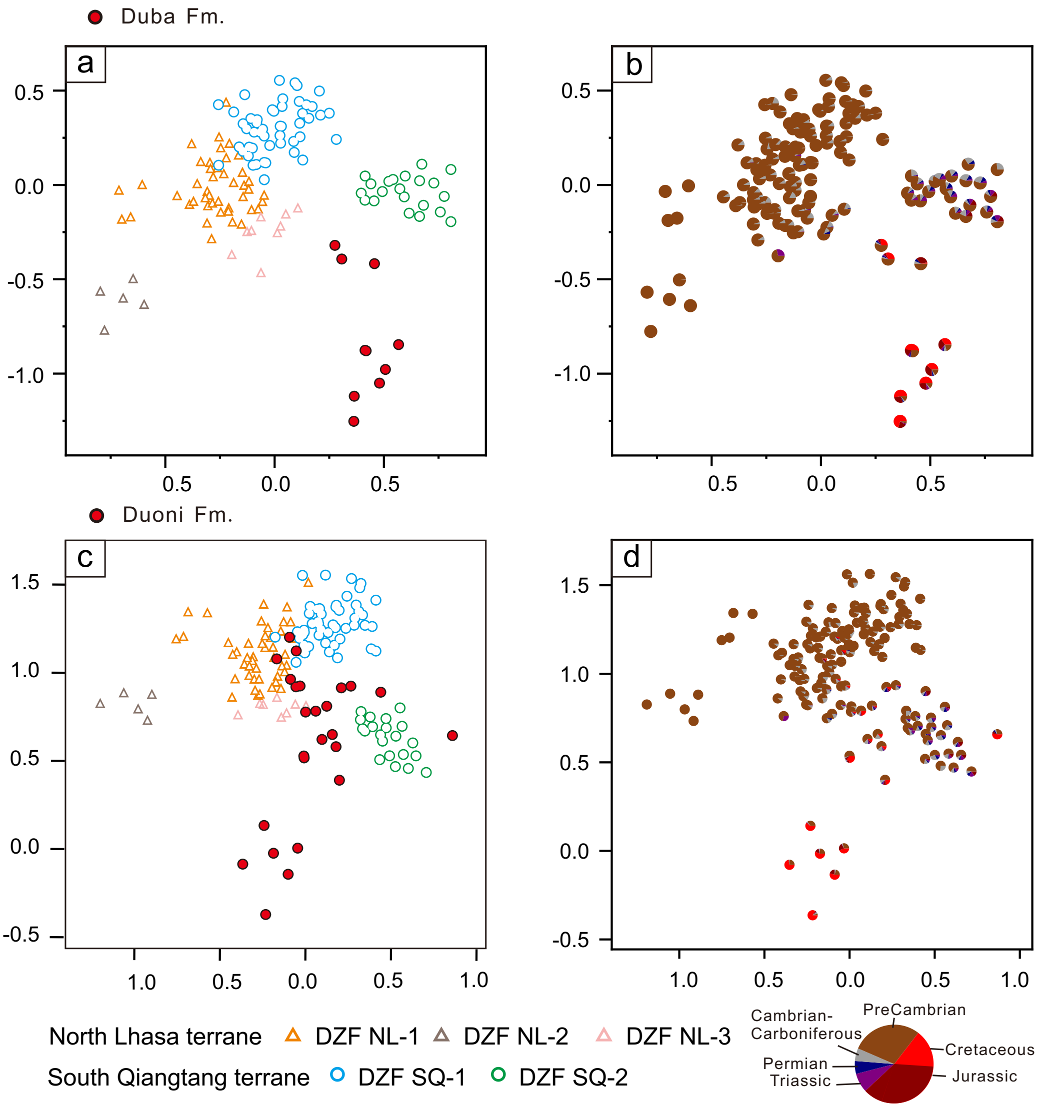
Duba Fm.
a
b
Duoni Fm.
c
d
North Lhasa terrane
DZF NL-1
DZF NL-2
DZF NL-3
South Qiangtang terrane
DZF SQ-1
DZF SQ-2
PreCambrian
Cambrian-Carboniferous
Permian
Triassic
Cretaceous
Jurassic

Fig.13

Table1 Detrital zircon age facies of the North Lhasa and South Qiangtang terranes

Terrane	Depositional age	DZF	Peak 1 (Ma)	Peak2 (Ma)	Peak3 (Ma)	Peak4 (Ma)	Number of samples
North Lhasa	PreT, T_3	DZF NL-1	538	978	1192		43
	PreT	DZF NL-2	1168				5
	T_3	DZF NL-3	304	558	1170		8
South Qiangtang	PreT、 T_1-T_2、 T_3-J	DZF SQ-1	547	793	956	2500	49
	T_3-J	DZF SQ-2	176	248	441	1861	21

Table 2 Detrital zircon age facies of the South Lhasa and Tethys Himalayan terranes

Terrane	Depositional age	DZF	Peak1 (Ma)	Peak2 (Ma)	Peak3 (Ma)	Peak4 (Ma)	Number of samples
South Lhasa	J-K	DZF SL-1	117	195	222	1171	40
	K	DZF SL-2	109				11
	K	DZF SL-3	92				14
Tethys Himalayan	PreT,J,K	DZF TH-1	529	933			36
	T3	DZF TH-2	234	520	583		48
	K1	DZF TH-3	127				3

Declaration of Competing Interest

The authors declare that they have no known competing financial interests or personal relationships that could have appeared to influence the work reported in this paper.

Table S2

Click here to access/download

Supplementary Material

Table S2 Zircon data for detritalPy after filtering.xlsx